# Supporting information for: Facile high-yield synthesis of unsymmetric end-off compartmental double Schiff-base ligands: easy access to mononuclear precursor and unsymmetric dinuclear complexes

Markus Schmidt, Helmar Görls, and Winfried Plass*

*Institut für Anorganische und Analytische Chemie, Friedrich-Schiller-Universität Jena, Humboldtstr. 8, 07743 Jena, Germany.*

E-mail: sekr.plass@uni-jena.de

Phone: +49 3641 948130. Fax: +49 3641 948132

Table S1: Crystallographic data and structure refinement parameters for [Ni(tsc-difo)$PPh_3$]·2MeOH and [$Zn_2$(tsc-hydra)$(OAc)_2$]·MeCN·$H_2O$

| | [Ni(tsc-difo)$PPh_3$]·2MeOH | [$Zn_2$(tsc-hydra)$(OAc)_2$]·MeCN·$H_2O$ |
|---|---|---|
| formula | $C_{30}H_{32}N_3NiO_4PS$ | $C_{30}H_{36}N_8O_6SZn_2$ |
| formula weight ($g\,mol^{-1}$) | 620.33 | 767.47 |
| color | brown | yellow |
| crystal size (mm) | 0.045 × 0.034 × 0.032 | 0.060 × 0.060 × 0.040 |
| crystal system | monoclinic | monoclinic |
| space group | $P2_1/n$ | $P2_1/n$ |
| $a$ (pm) | 1483.10(6) | 1347.46(8) |
| $b$ (pm) | 767.72(3) | 1502.26(11) |
| $c$ (pm) | 2582.78(9) | 1667.45(12) |
| $\alpha$ (°) | 90 | 90 |
| $\beta$ (°) | 93.346(1) | 93.667(4) |
| $\gamma$ (°) | 90 | 90 |
| $V$ ($10^6$ $pm^3$) | 2935.75(19) | 3368.4(4) |
| $Z$ | 4 | 4 |
| $T$ (K) | 133(2) | 133(2) |
| $\rho_{calc}$ ($g\,cm^{-3}$) | 1.403 | 1.513 |
| $F(000)$ | 1296 | 1584 |
| $\mu$(Mo $K_\alpha$) ($mm^{-1}$) | 0.826 | 1.540 |
| $\Theta$ range of data collection (°) | 2.67−27.45 | 2.42−27.49 |
| measured reflections | 16312 | 15345 |
| unique reflections ($R_{int}$) | 6439 (0.0333) | 6769 (0.0447) |
| no. of parameters | 450 | 457 |
| goodness-of-fit on $F^2$ | 1.124 | 1.177 |
| $R1$ ($I > 2\sigma(I)$) | 0.0478 | 0.0565 |
| $wR2$ (all data) | 0.1226 | 0.1176 |

Table S2: Selected $^{13}C$ NMR data for mono and double Schiff bases ($\delta$/ppm)

| Ligand | C1 | C2 | C3 | C4 | C5 | C6 | C7 | C8 | C9 | C10 |
|---|---|---|---|---|---|---|---|---|---|---|
| $H_2$sc-difo | 156.3 | 135.5 | 122.2 | 134.1 | 128.8 | 132.3 | 121.9 | 156.4 | 19.7 | 194.6 |
| $H_2$tsc-difo | 177.9 | 137.1 | 122.1 | 134.2 | 129.1 | 134.3 | 121.8 | 156.7 | 19.7 | 195.7 |
| $H_2$sc-hydra | 156.8 | 134.6 | 122.3 | 128.9 | 126.2 | 132.7 | 118.2 | 158.8 | 20.0 | 166.5 |
| $H_2$tsc-hydra | 177.7 | 137.8 | 121.9 | 129.7 | 125.9 | 133.7 | 118.0 | 160.5 | 19.9 | 166.5 |
| $H_2$sc-ampy | 156.8 | 134.2 | 121.0 | 129.0 | 127.0 | 132.9 | 118.5 | 157.6 | 19.9 | 167.5 |
| $H_2$tsc-ampy | 177.8 | 137.3 | 121.5 | 129.4 | 126.9 | 133.9 | 118.5 | 158.6 | 19.9 | 167.5 |
| $H_3$sc-amph | 156.8 | 134.4 | 122.1 | 129.3 | 127.1 | 133.4 | 119.3 | 157.6 | 20.0 | 161.4 |
| $H_3$tsc-amph | 177.8 | 137.4 | 121.6 | 129.8 | 127.1 | 134.3 | 119.3 | 158.6 | 20.0 | 161.3 |

Table S3: Bond angles at the nickel(II) ion in the crystal structure of [Ni(tsc-difo)$PPh_3$]·2MeOH (in deg)

| | |
|---|---|
| S–Ni–P | 91.46(3) |
| S–Ni–O1 | 174.29(7) |
| P–Ni–O1 | 86.39(6) |
| O1–Ni–N3 | 95.13(10) |
| S–Ni–N3 | 87.33(8) |
| P–Ni–N3 | 176.35(8) |

Table S4: Bond angles at the zinc(II) ions in the crystal structure of [$Zn_2$(tsc-hydra)$(OAc)_2$]·MeCN·$H_2O$ (in deg)

| | | | |
|---|---|---|---|
| S–Zn1–O1 | 150.00(9) | O1–Zn2–O4 | 75.22(11) |
| S–Zn1–O2 | 115.13(10) | O1–Zn2–N4 | 85.40(12) |
| S–Zn1–O4 | 100.29(9) | O1–Zn2–N5 | 161.90(12) |
| S–Zn1–N3 | 82.40(10) | O1–Zn2–N6 | 113.57(13) |
| O1–Zn1–O2 | 94.40(13) | O1–Zn2–N7 | 96.30(13) |
| O1–Zn1–O4 | 76.00(11) | O4–Zn2–N4 | 155.62(13) |
| O1–Zn1–N3 | 84.53(12) | O4–Zn2–N5 | 121.10(12) |
| O2–Zn1–O4 | 104.21(13) | O4–Zn2–N6 | 87.48(13) |
| O2–Zn1–N3 | 105.96(13) | O4–Zn2–N7 | 93.62(13) |
| O4–Zn1–N3 | 145.09(13) | N4–Zn2–N5 | 80.55(13) |
| | | N4–Zn2–N6 | 86.87(15) |
| | | N4–Zn2–N7 | 103.22(15) |
| | | N5–Zn2–N6 | 77.15(14) |
| | | N6–Zn2–N7 | 76.06(14) |
| | | N6–Zn2–N7 | 149.27(14) |

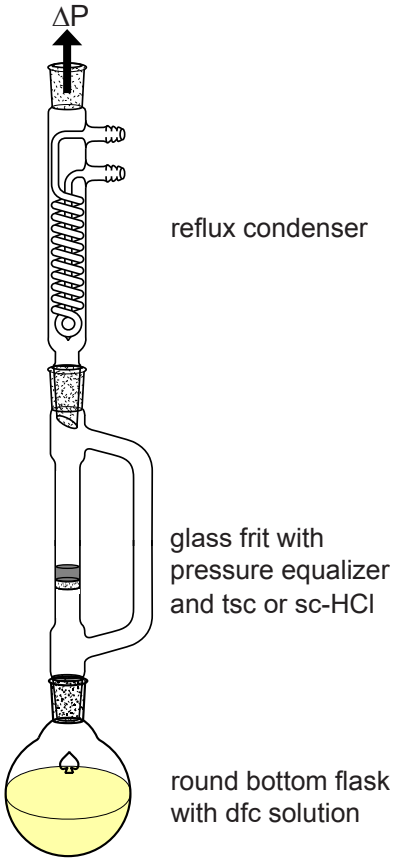


Figure S1: Experimental setup for the synthesis of the proligands $H_2$sc-difo and $H_2$tsc-difo in gram scale and high purity.

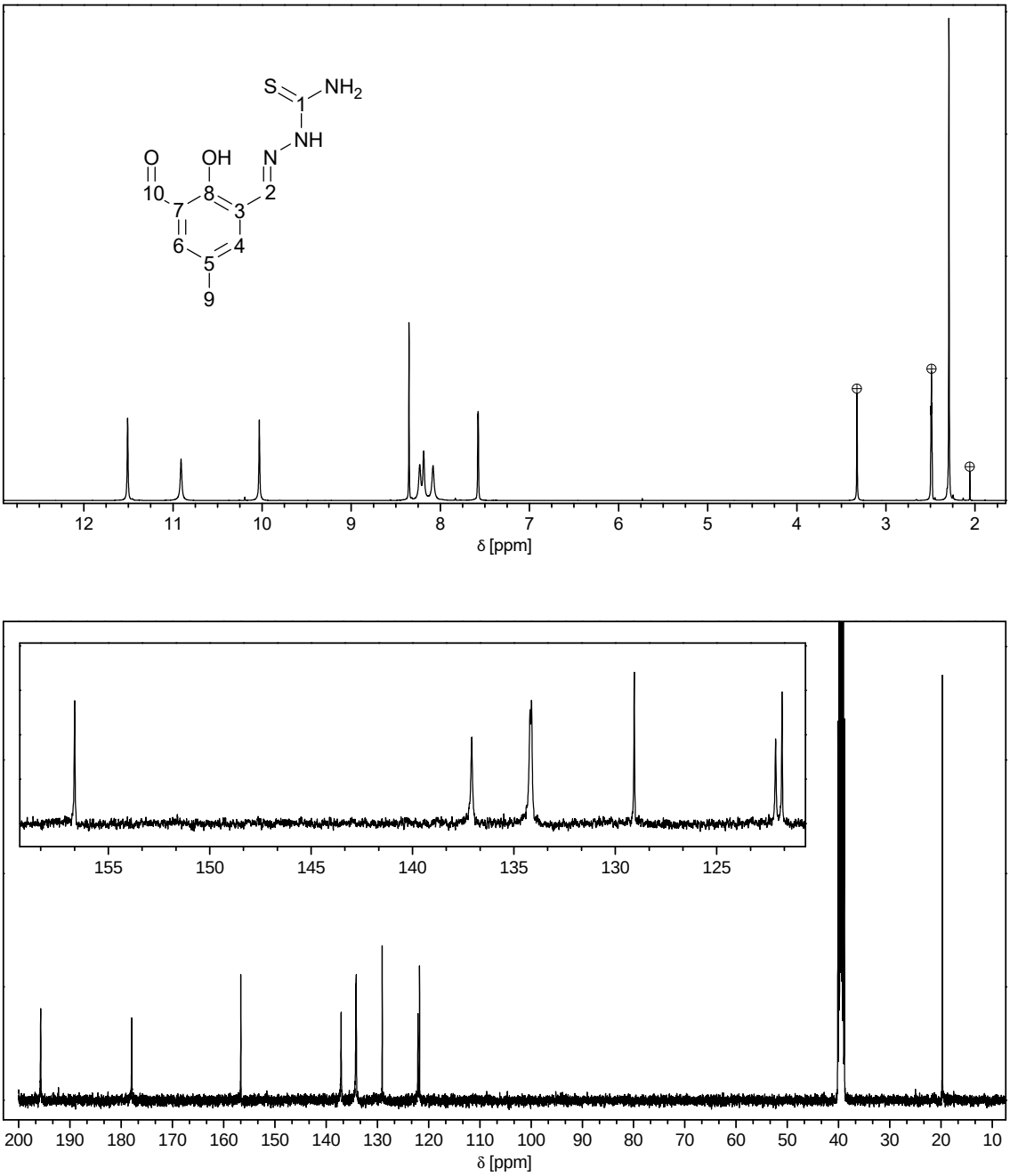


Figure S2: NMR spectra of $H_2$tsc-difo in DMSO-$d_6$: (Top) $^1$H NMR; marked peaks correspond to water, acetonitrile and DMSO. (Bottom) $^{13}$C{$^1$H} NMR.

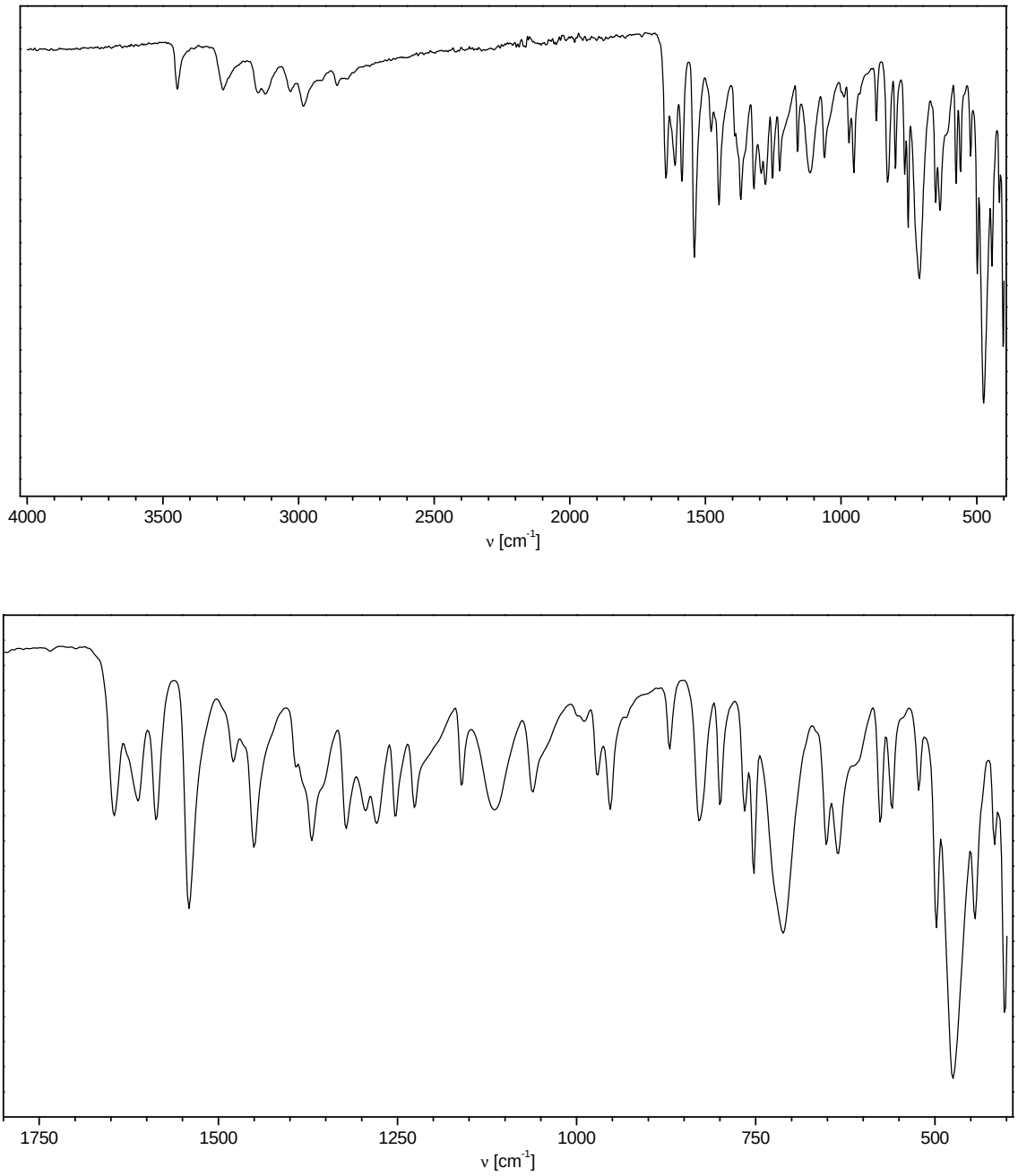


Figure S3: FT-IR spectra of $H_2$tsc-difo: (Top) Overview range from 4000–400 $cm^{-1}$. (Bottom) Fingerprint region from 1800–400 $cm^{-1}$. List of the positions of vibrational bands (in $cm^{-1}$): 3447, 3278, 3150, 3124, 3034, 2981, 2857, 1644, 1614, 1584, 1540, 1480, 1448, 1370, 1319, 1277, 1251, 1223, 1159, 1112, 1058, 971, 952, 872, 827, 798, 767, 753, 714, 650, 634, 577, 560, 521, 478, 444, 415, 404.

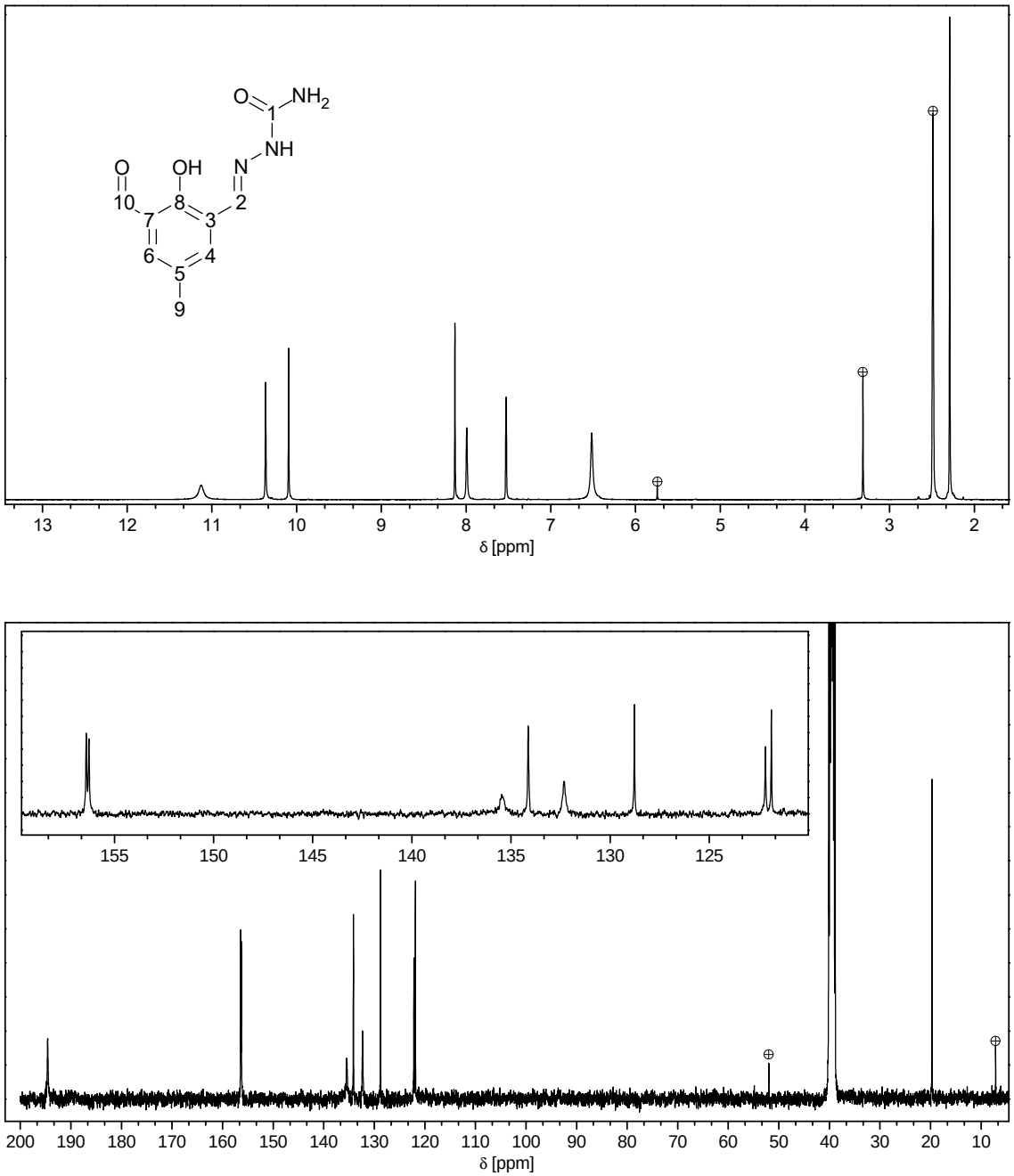


Figure S4: NMR spectra of $H_2$tsc-difo in DMSO-$d_6$: (Top) $^1$H NMR; marked peaks correspond to water, dichloromethane and DMSO. (Bottom) $^{13}C\{^1H\}$ NMR; marked peaks correspond diethyl ether.

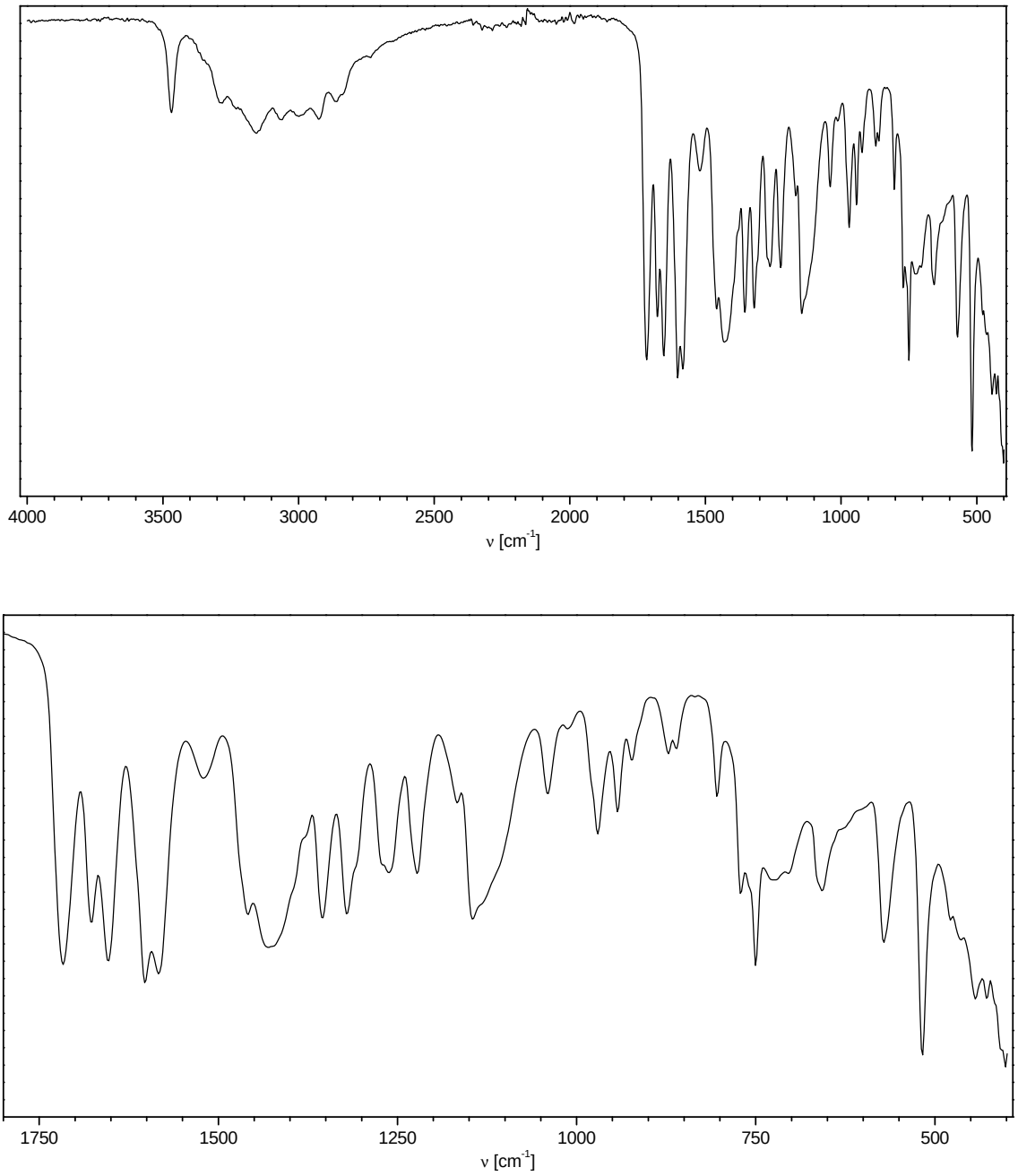


Figure S5: FT-IR spectra of $H_2$sc-difo: (Top) Overview range from 4000–400 $cm^{-1}$. (Bottom) Fingerprint region from 1800–400 $cm^{-1}$. List of the positions of vibrational bands (in $cm^{-1}$): 3469, 3288, 3158, 3064, 2998, 2922, 2865, 1714, 1675, 1652, 1602, 1582, 1517, 1463, 1428, 1355, 1321, 1261, 1222, 1170, 1145, 1039, 968, 941, 923, 875, 858, 804, 772, 751, 724, 657, 573, 518, 445, 401.

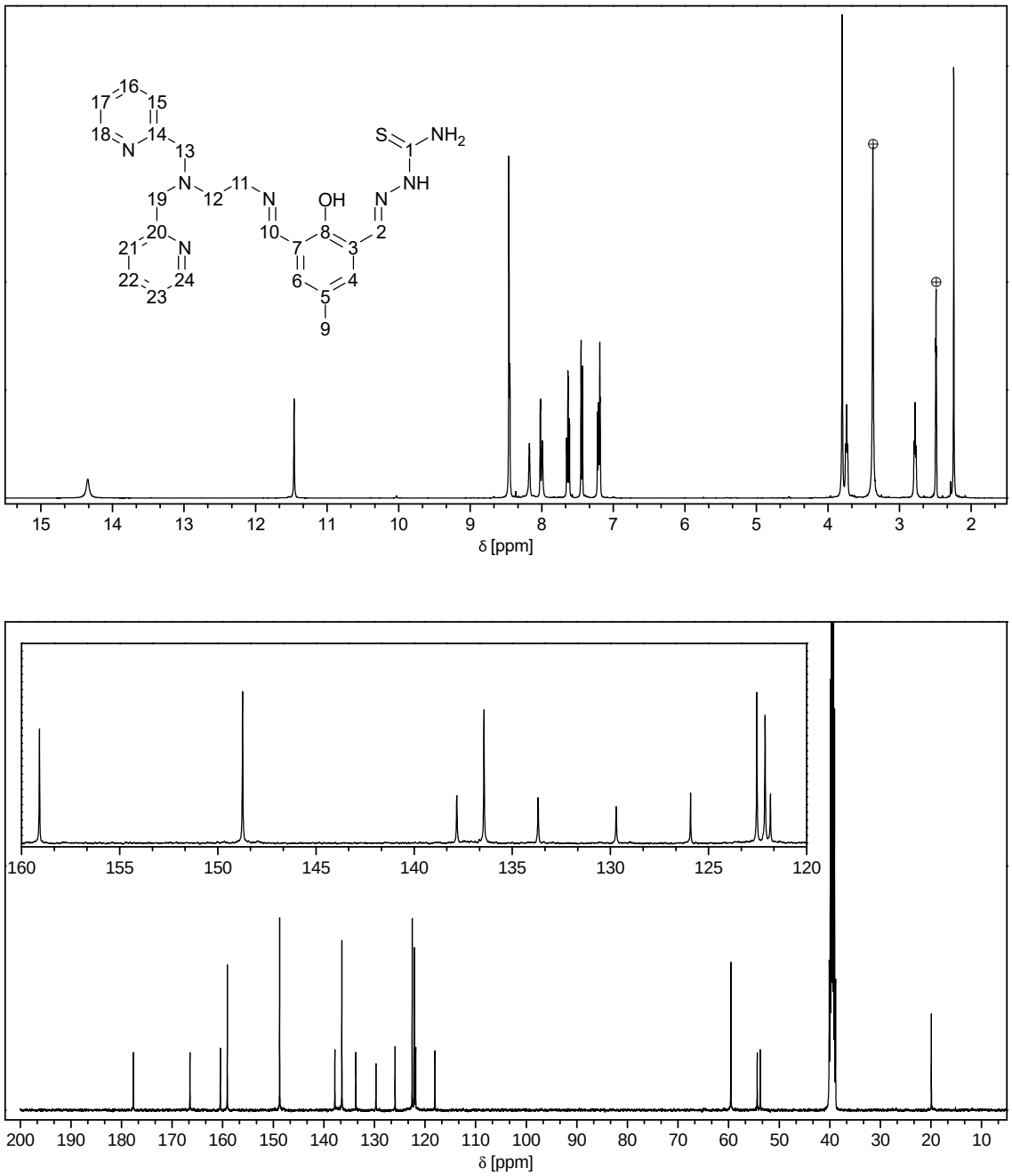


Figure S6: NMR spectra of $H_2$tsc-hydra in DMSO-$d_6$: (Top) $^1$H NMR; marked peaks correspond to water and DMSO. (Bottom) $^{13}$C{$^1$H} NMR.

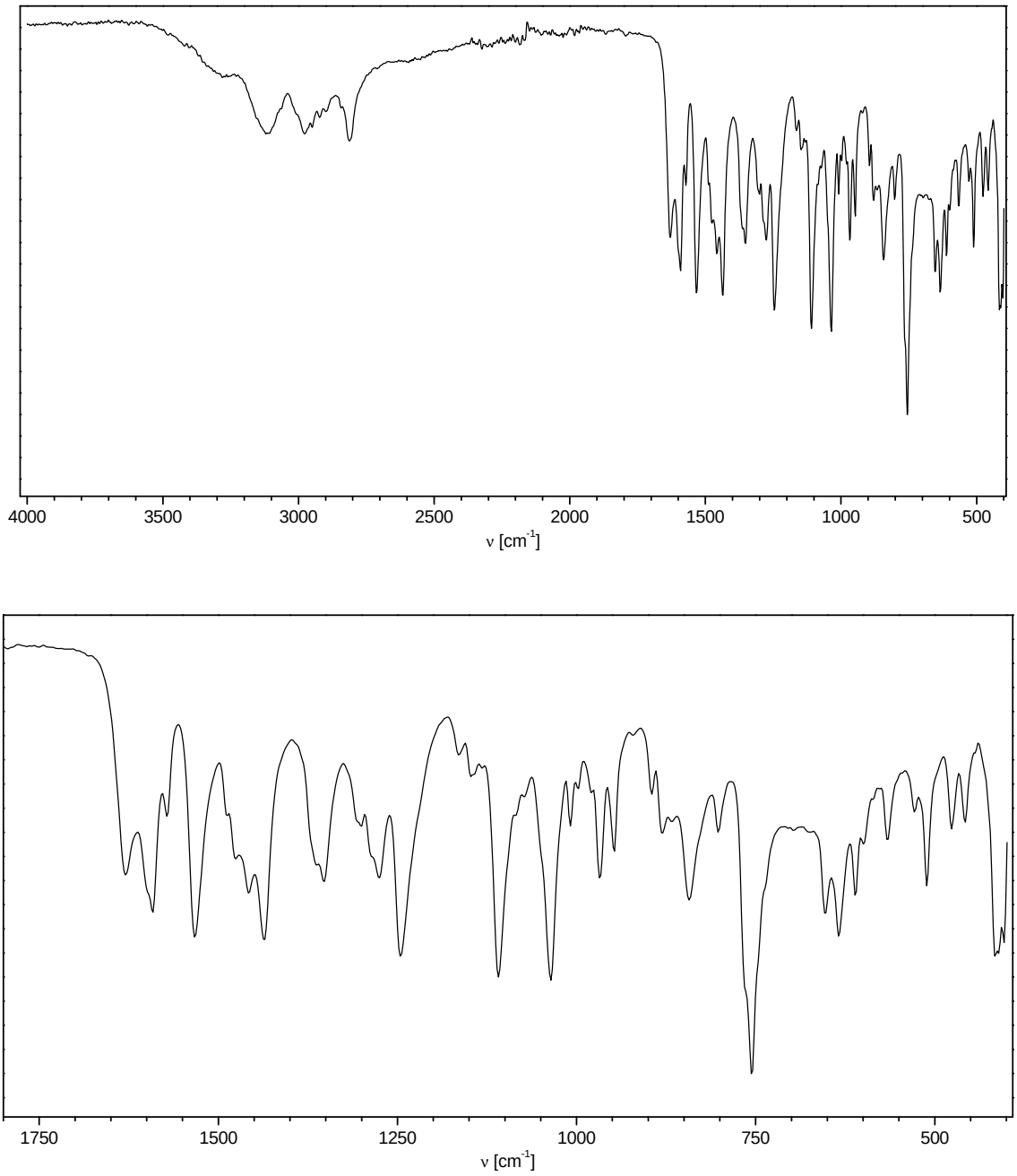


Figure S7: FT-IR spectra of $H_2$tsc-hydra: (Top) Overview range from 4000–400 $cm^{-1}$. (Bottom) Fingerprint region from 1800–400 $cm^{-1}$. List of the positions of vibrational bands (in $cm^{-1}$): 3117, 2977, 2947, 2922, 2895, 2810, 1630, 1591, 1570, 1531, 1456, 1435, 1364, 1353, 1305, 1275, 1247, 1165, 1145, 1108, 1035, 1010, 968, 948, 898, 879, 843, 801, 753, 653, 637, 611, 566, 529, 513, 477, 458, 420.

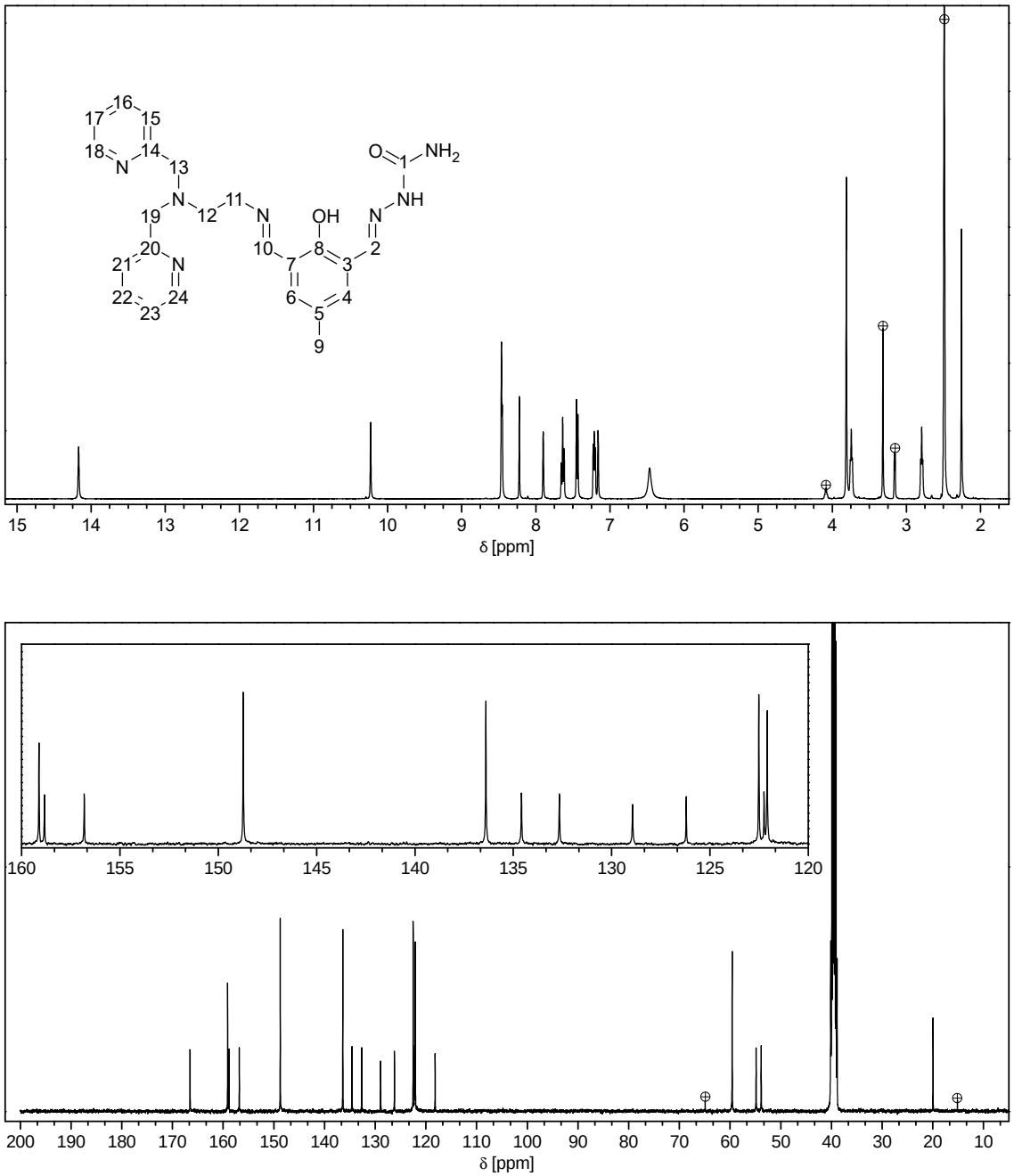


Figure S8: NMR spectra of $H_2$sc-hydra in DMSO-$d_6$: (Top) $^1$H NMR; marked peaks correspond to water, methanol and DMSO. (Bottom) $^{13}$C{$^1$H} NMR; marked peaks are assigned to diethyl ether.

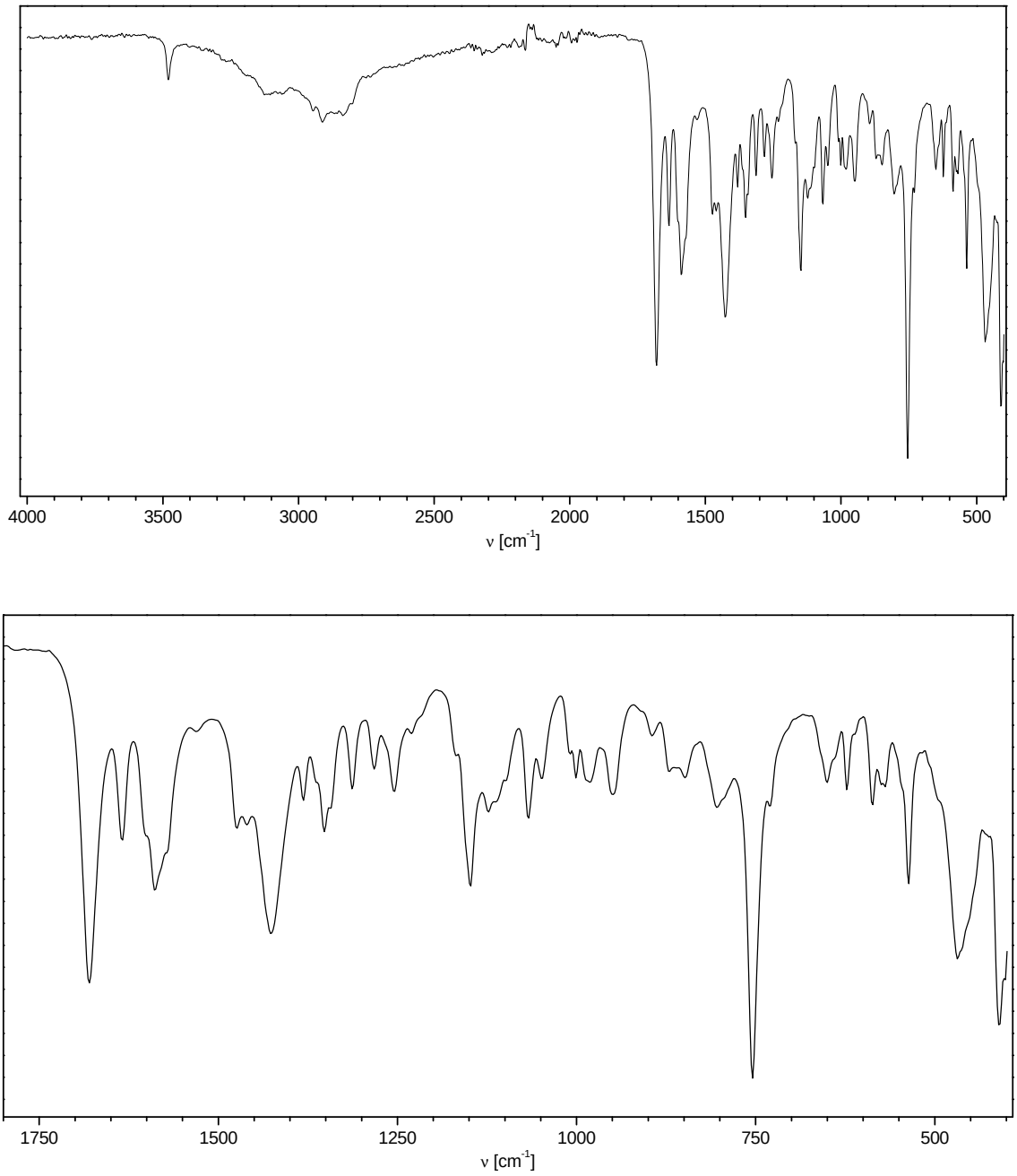


Figure S9: FT-IR spectra of $H_2$sc-hydra: (Top) Overview range from 4000–400 $cm^{-1}$. (Bottom) Fingerprint region from 1800–400 $cm^{-1}$. List of the positions of vibrational bands (in $cm^{-1}$): 3480, 3124, 3064, 2945, 2918, 2833, 1680, 1634, 1591, 1474, 1460, 1428, 1383, 1353, 1312, 1282, 1252, 1229, 1147, 1122, 1065, 1046, 1005, 984, 948, 898, 872, 849, 808, 756, 730, 650, 625, 589, 570, 538, 470, 412.

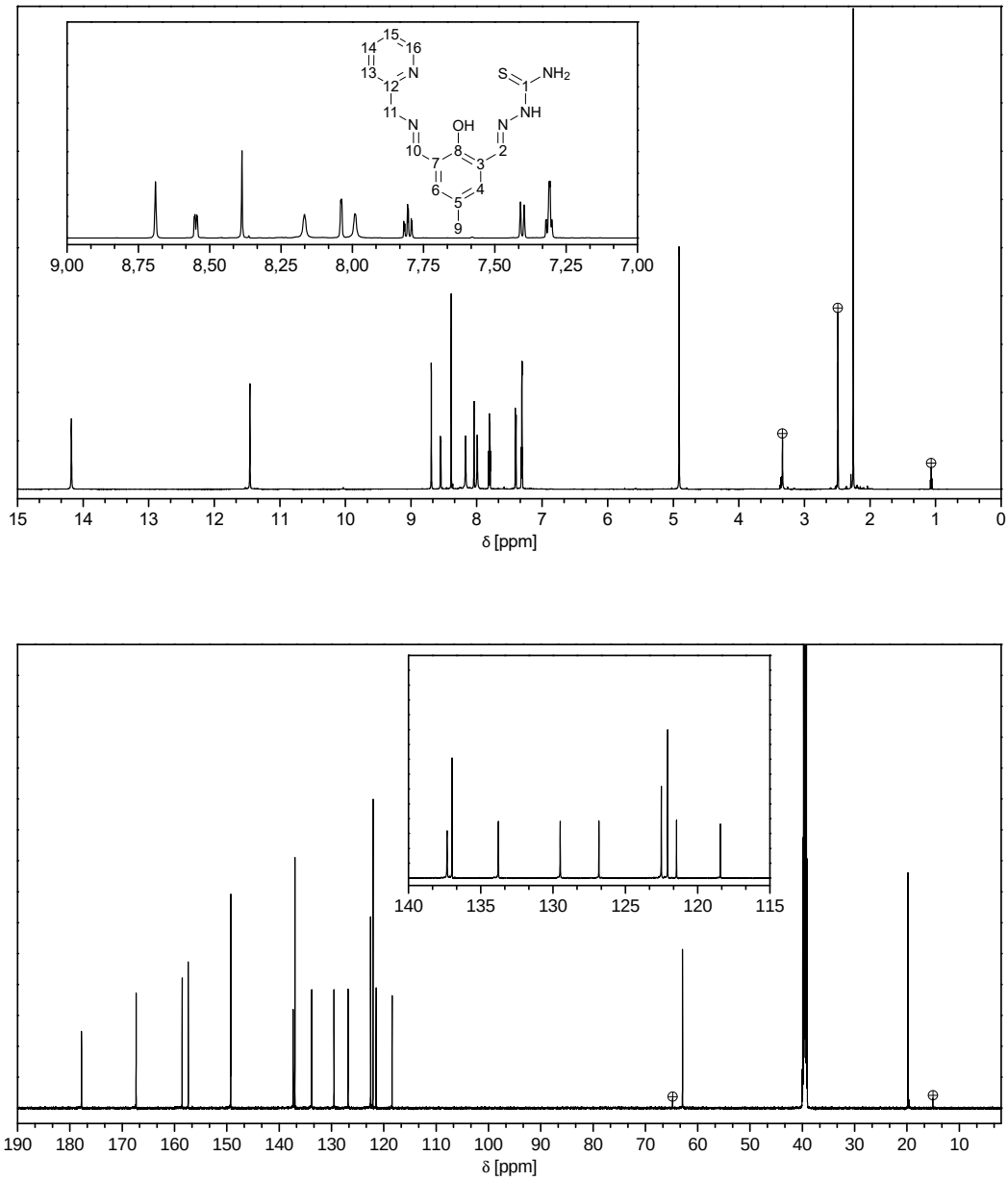


Figure S10: NMR spectra of $H_2$tsc-ampy in DMSO-$d_6$: (Top) $^1$H NMR; marked peaks correspond to water, DMSO and diethyl ether. (Bottom) $^{13}$C{$^1$H} NMR; marked peaks correspond to diethyl ether.

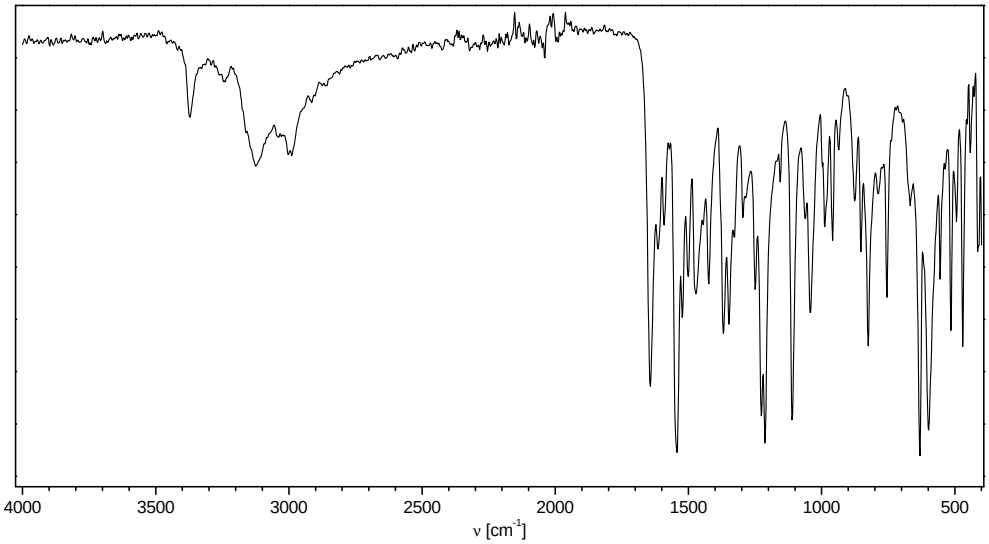


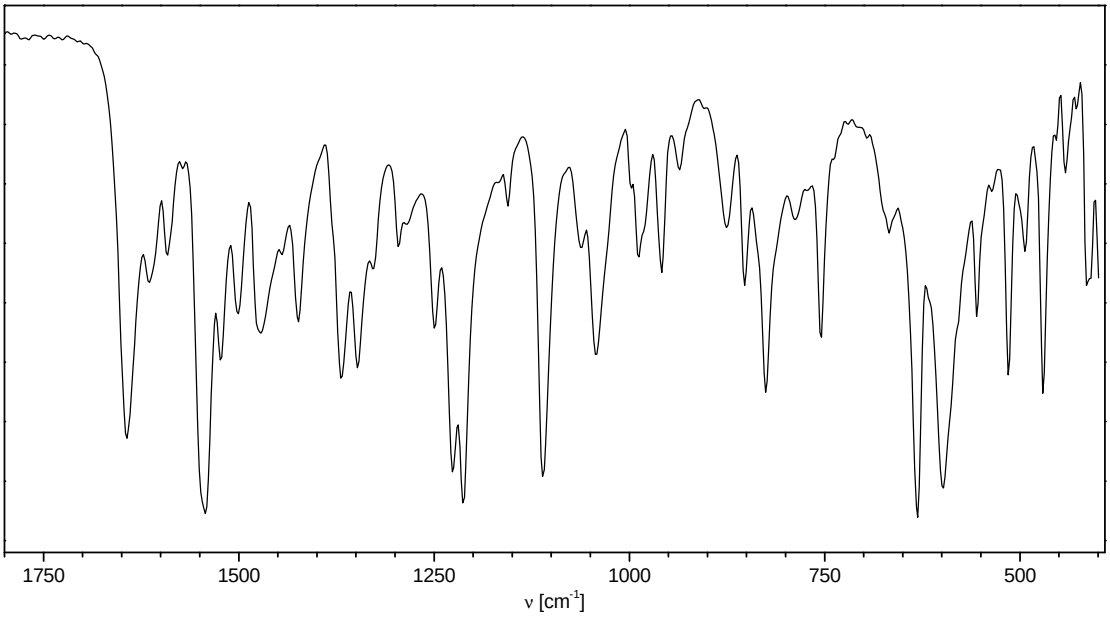


Figure S11: FT-IR spectra of $H_2$tsc-ampy: (Top) Overview range from 4000–400 $cm^{-1}$. (Bottom) Fingerprint region from 1800–400 $cm^{-1}$. List of the positions of vibrational bands (in $cm^{-1}$): 3374, 3125, 2992, 1640, 1612, 1588, 1544, 1522, 1499, 1471, 1422, 1368, 1347, 1295, 1248, 1227, 1211, 1154, 1108, 1065, 1042, 986, 960, 937, 873, 854, 826, 756, 669, 632, 599, 557, 515, 493, 470, 414.

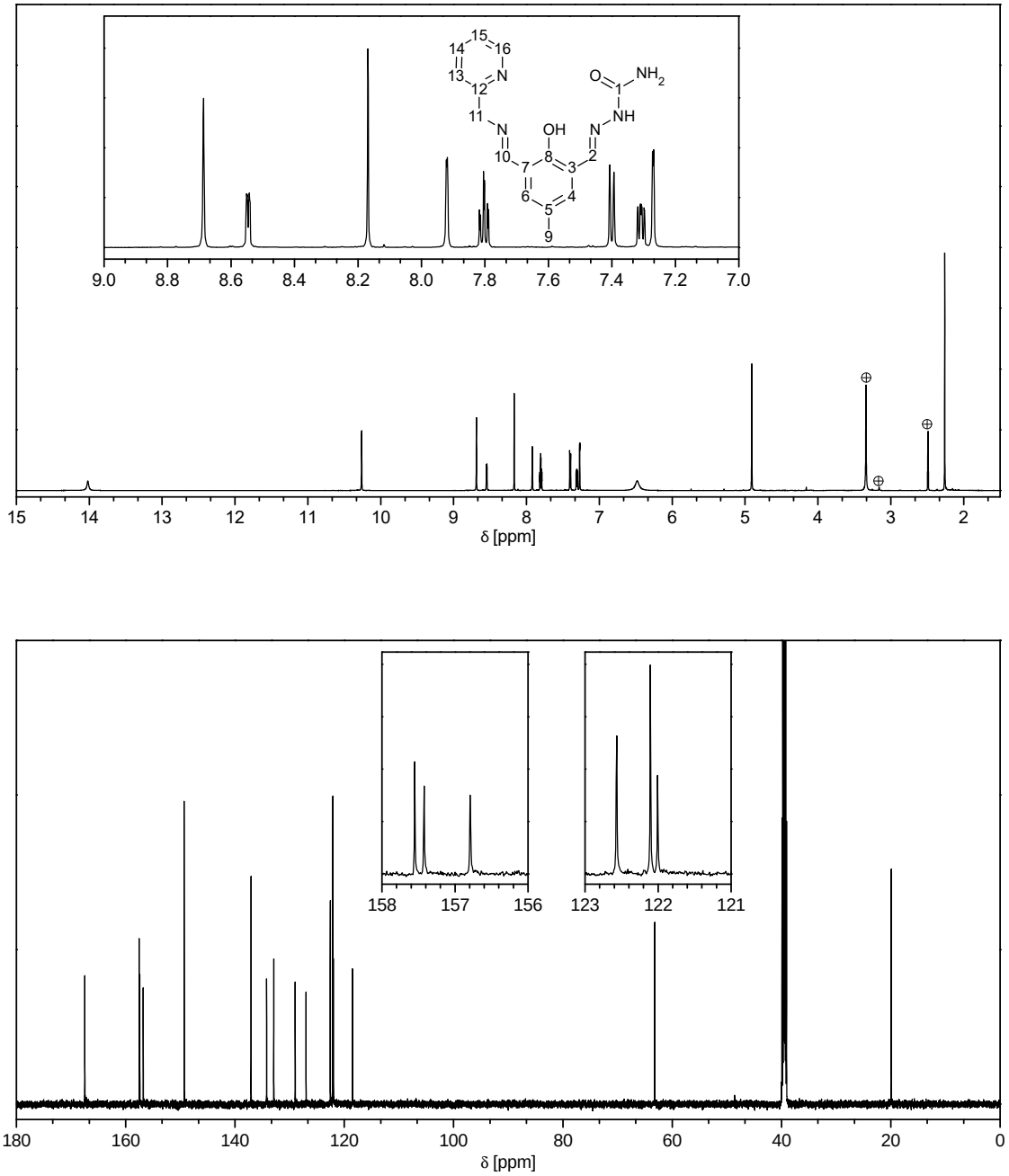


Figure S12: NMR spectra of $H_2$sc-ampy in DMSO-$d_6$: (Top) $^1$H NMR; marked peaks correspond to water, methanol and DMSO. (Bottom) $^{13}$C{$^1$H} NMR.

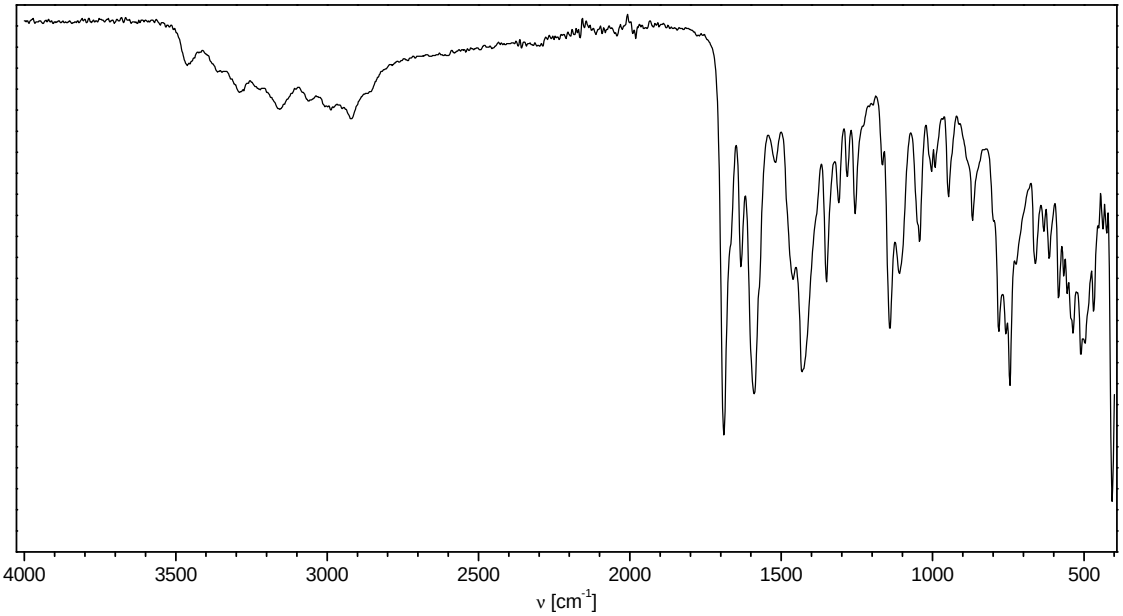


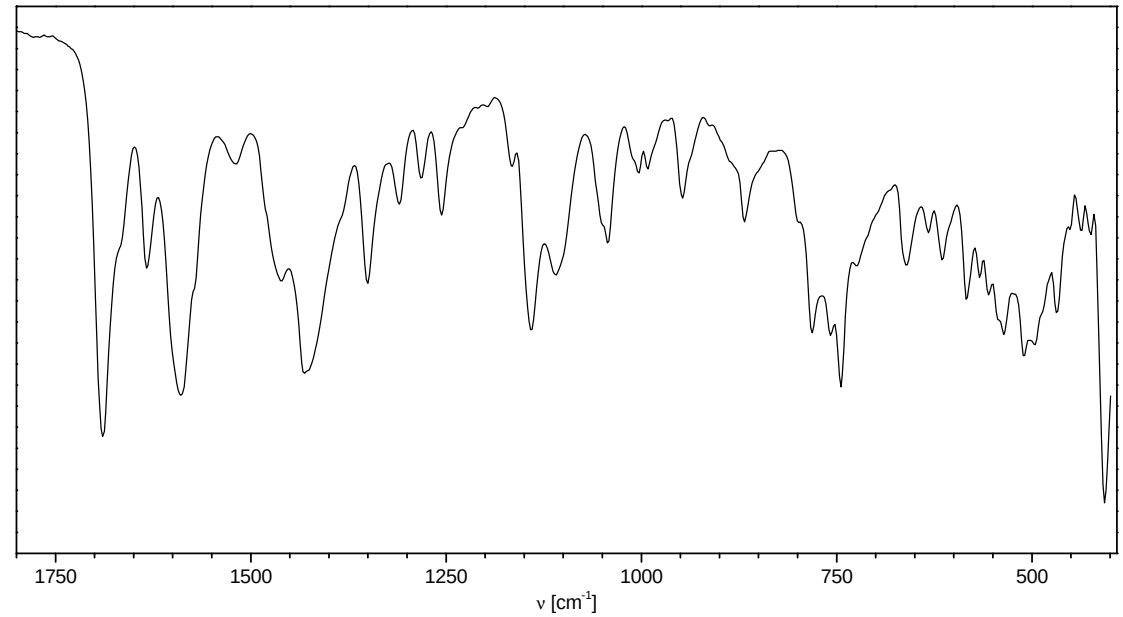


Figure S13: FT-IR spectra of $H_2$sc-ampy: (Top) Overview range from 4000–400 $cm^{-1}$. (Bottom) Fingerprint region from 1800–400 $cm^{-1}$. List of the positions of vibrational bands (in $cm^{-1}$): 3465, 3286, 3154, 2918, 1688, 1635, 1587, 1521, 1465, 1426, 1350, 1310, 1282, 1261, 1141, 1103, 1040, 1007, 991, 948, 869, 780, 742, 722, 661, 635, 617, 582, 538, 508, 495, 467.

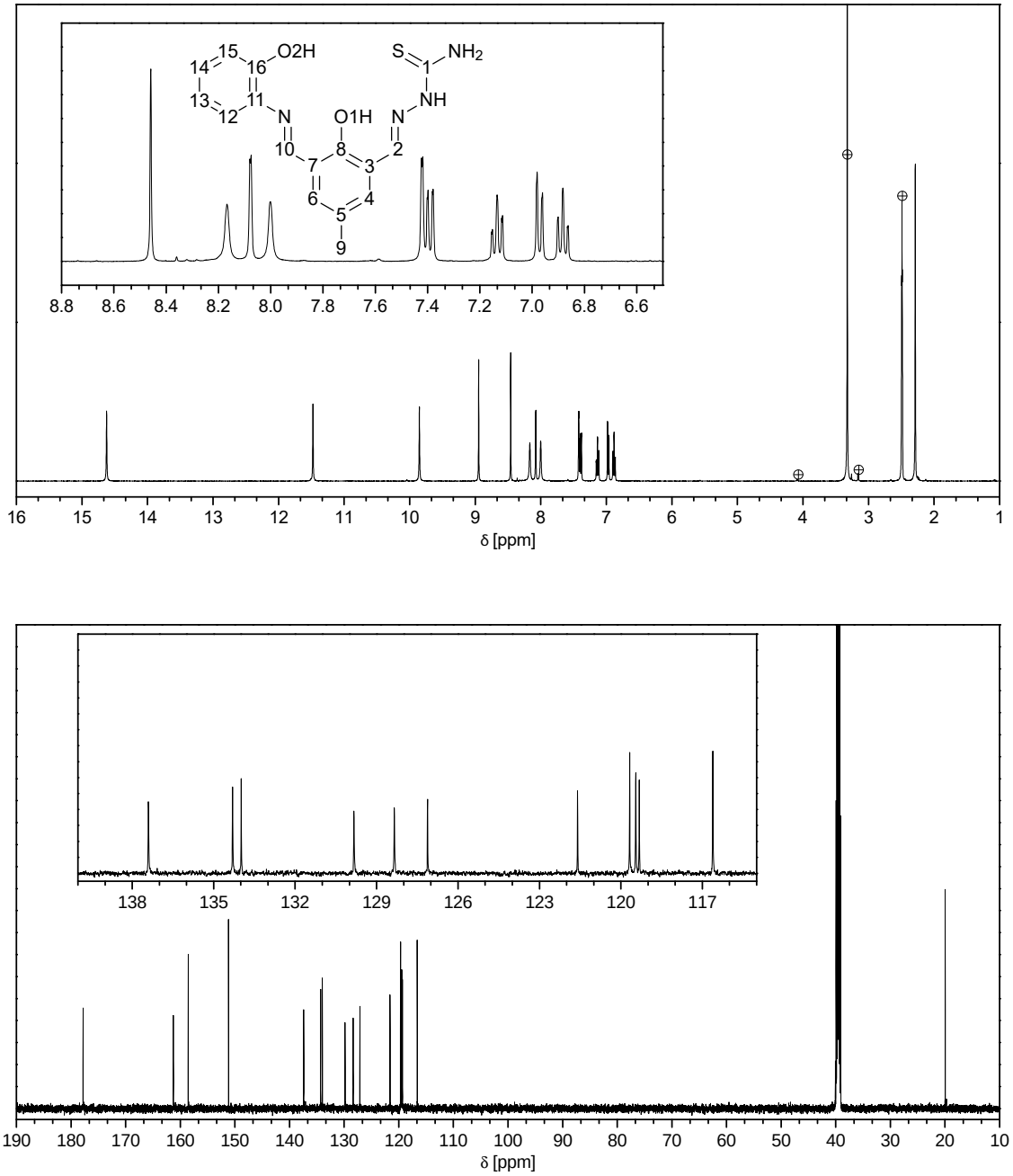


Figure S14: NMR spectra of $H_3$tsc-amph in DMSO-$d_6$: (Top) $^1$H NMR; marked peaks correspond to water, methanol and DMSO. (Bottom) $^{13}$C{$^1$H} NMR.

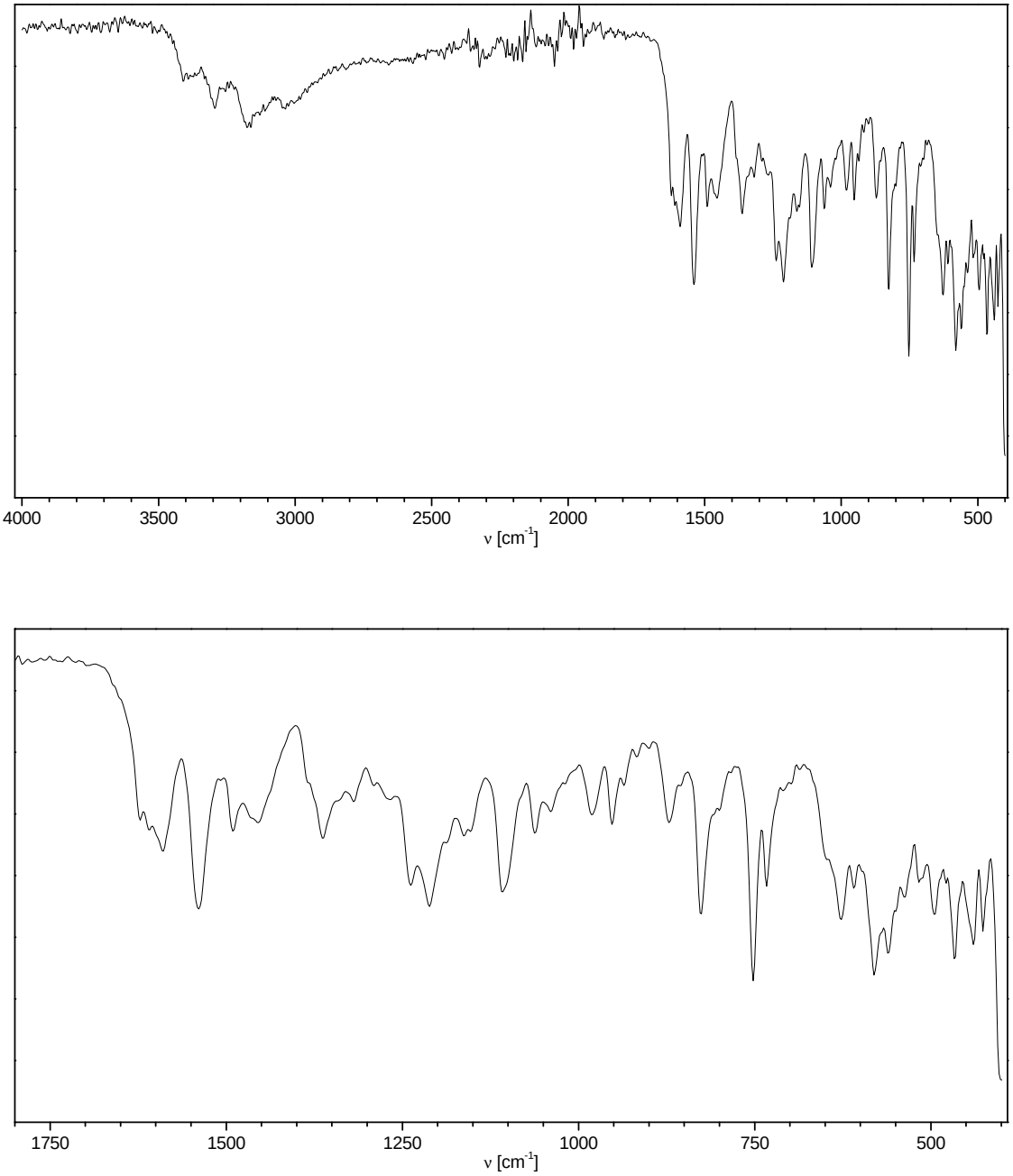


Figure S15: FT-IR spectra of $H_3$tsc-amph: (Top) Overview range from 4000–400 $cm^{-1}$. (Bottom) Fingerprint region from 1800–400 $cm^{-1}$. List of the positions of vibrational bands (in $cm^{-1}$): 3411, 3294, 3177, 1589, 1541, 1490, 1457, 1363, 1320, 1238, 1213, 1159, 1106, 1065, 1035, 979, 951, 935, 874, 828, 750, 732, 625, 605, 582, 561, 538, 495, 473, 439, 424.

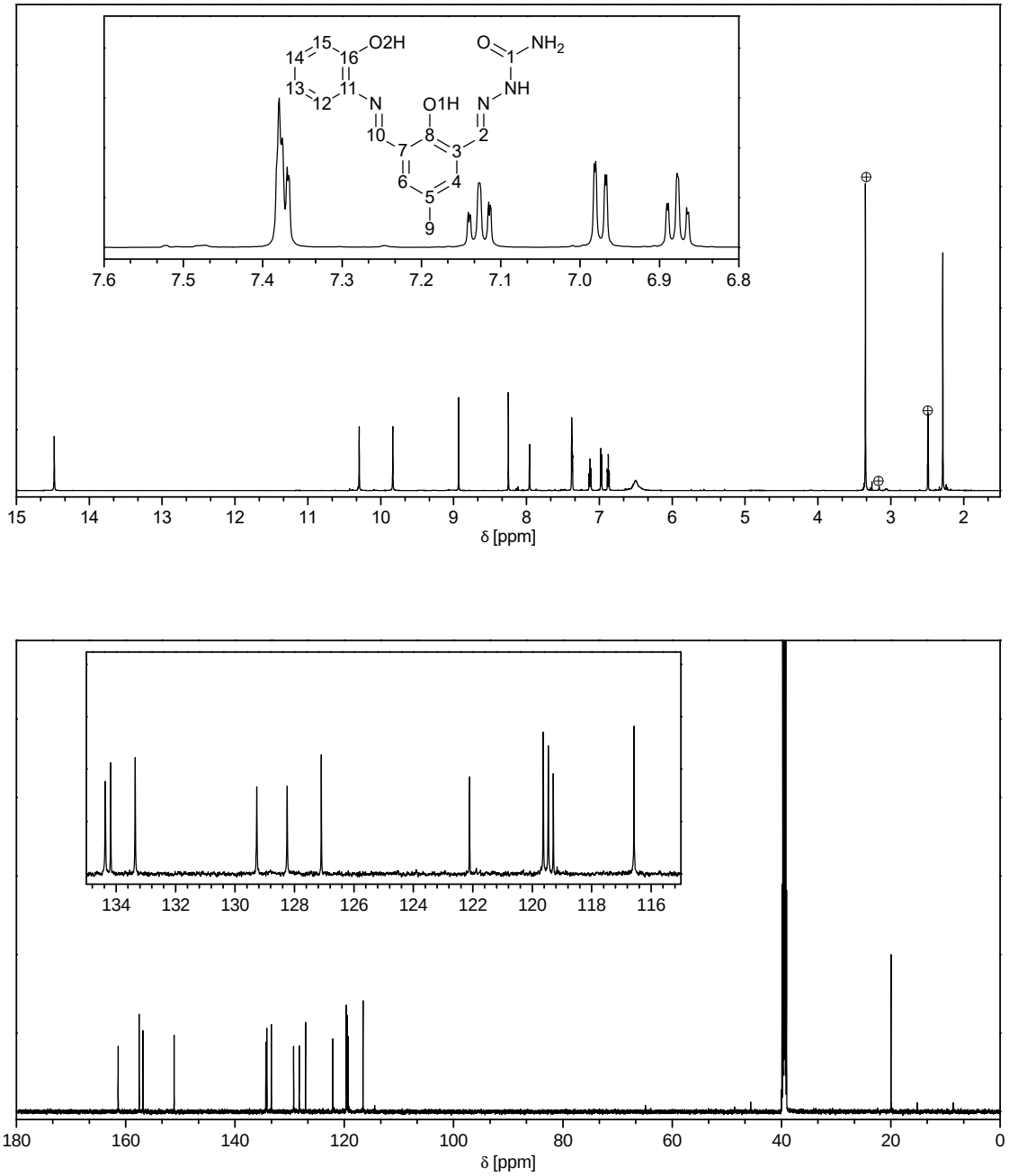


Figure S16: NMR spectra of $H_3$sc-amph in DMSO-$d_6$: (Top) $^1$H NMR; marked peaks correspond to water, methanol and DMSO. (Bottom) $^{13}$C{$^1$H} NMR.

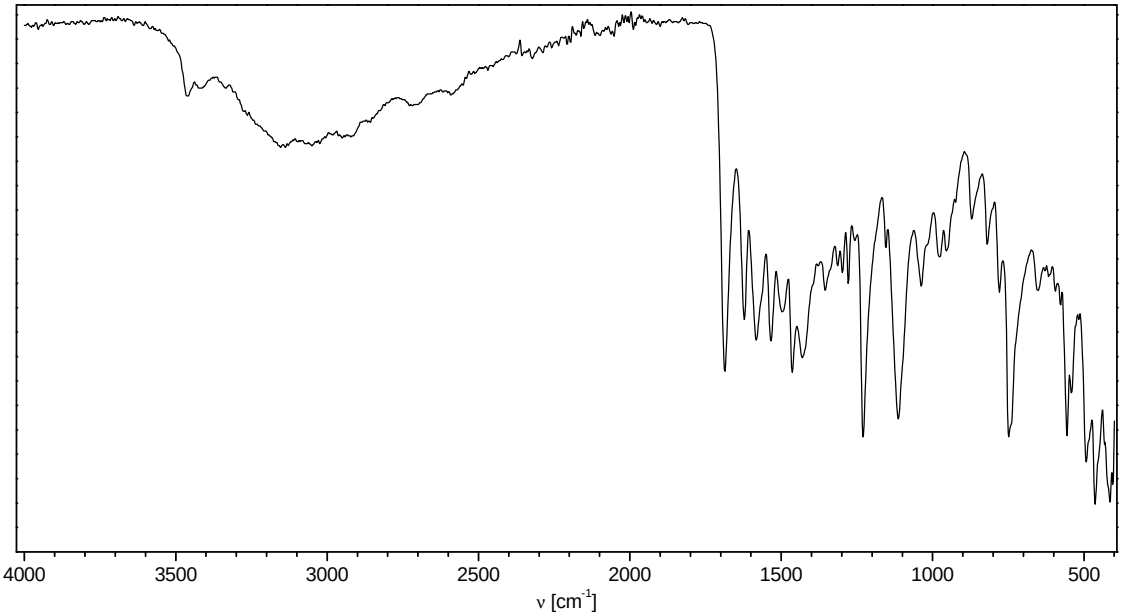


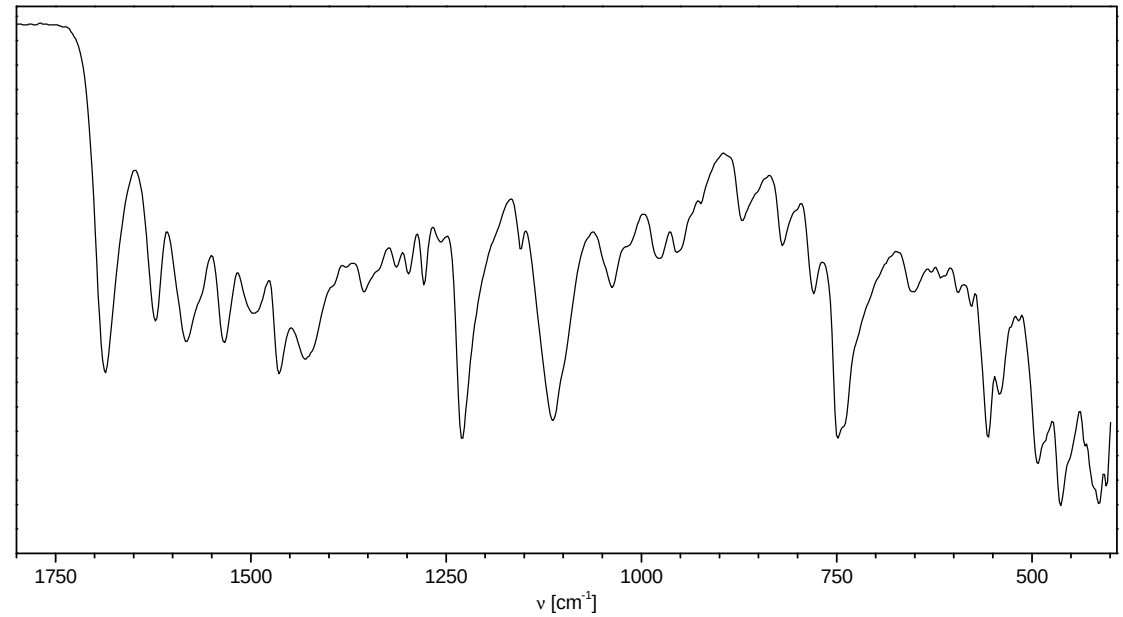


Figure S17: FT-IR spectra of $H_3$sc-amph: (Top) Overview range from 4000–400 $cm^{-1}$. (Bottom) Fingerprint region from 1800–400 $cm^{-1}$. List of the positions of vibrational bands (in $cm^{-1}$): 3470, 3146, 3047, 2700, 1683, 1620, 1579, 1533, 1500, 1465, 1434, 1355, 1282, 1231, 1157, 1111, 1035, 976, 956, 872, 821, 783, 750, 656, 556, 541, 493, 462, 414.

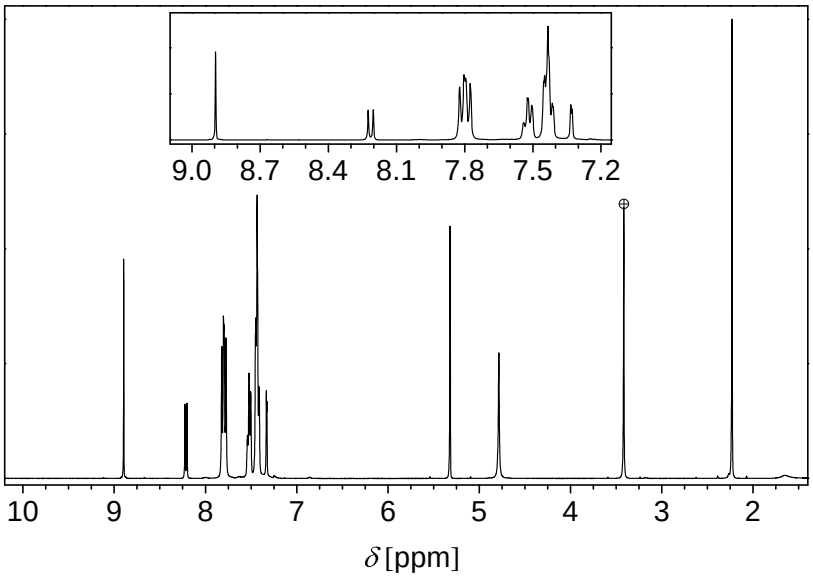


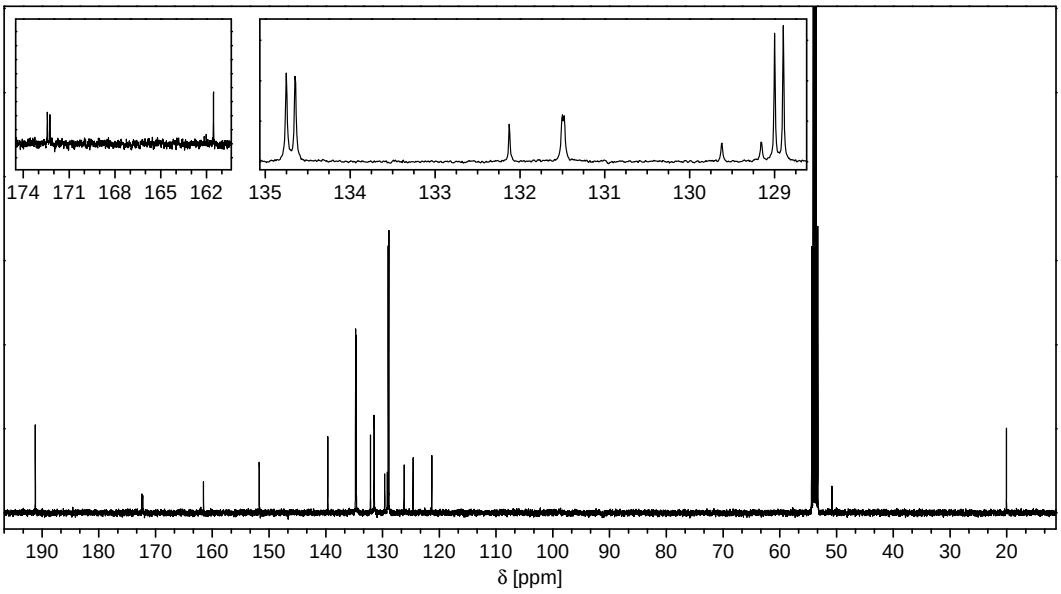


Figure S18: NMR spectra of [Ni(tsc-difo)$PPh_3$] in $CD_2Cl_2$: (Top) $^1$H NMR; marked peak corresponds to methanol which is included in the crystal packing. (Bottom) $^{13}$C{$^1$H} NMR. For notation of the ligand atoms cf. Fig. S2.

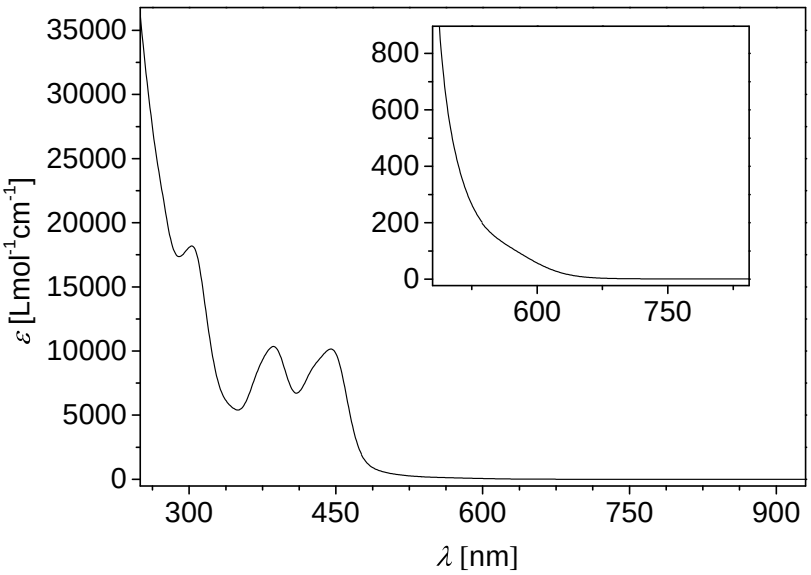


Figure S19: UV/Vis spectrum of [Ni(tsc-difo)$PPh_3$] in dichloromethane.

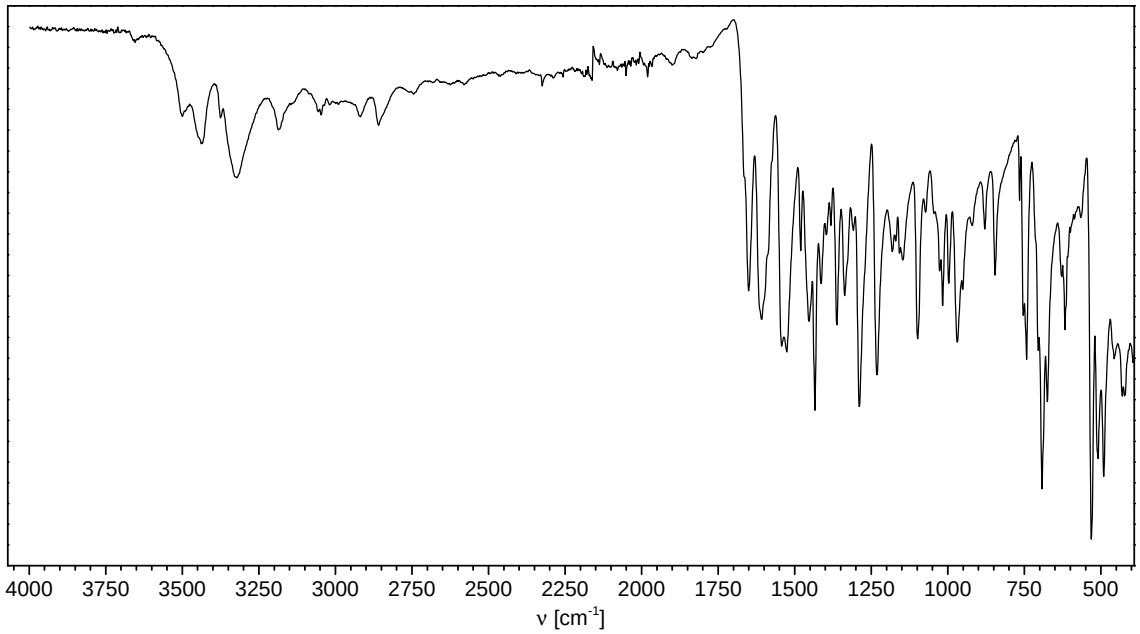


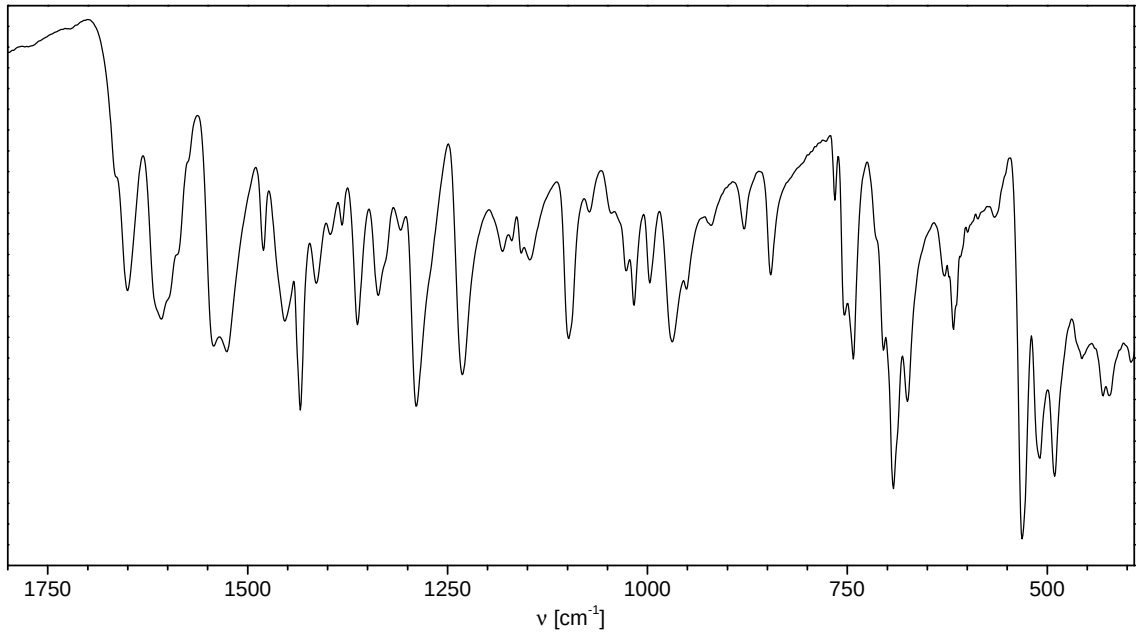


Figure S20: FT-IR spectra of [Ni(tsc-difo)$PPh_3$]: (Top) Overview range from 4000–400 $cm^{-1}$. (Bottom) Fingerprint region from 1800–400 $cm^{-1}$. List of the positions of vibrational bands (in $cm^{-1}$): 3503, 3438, 3375, 3324, 3182, 3047, 2916, 2858, 1649, 1603, 1545, 1526, 1480, 1454, 1434, 1413, 1396, 1381, 1362, 1335, 1309, 1287, 1229, 1181, 1145, 1099, 1072, 1026, 1014, 997, 966, 952, 920, 877, 843, 766, 754, 742, 693, 674, 616, 565, 531, 507, 488, 457, 428.

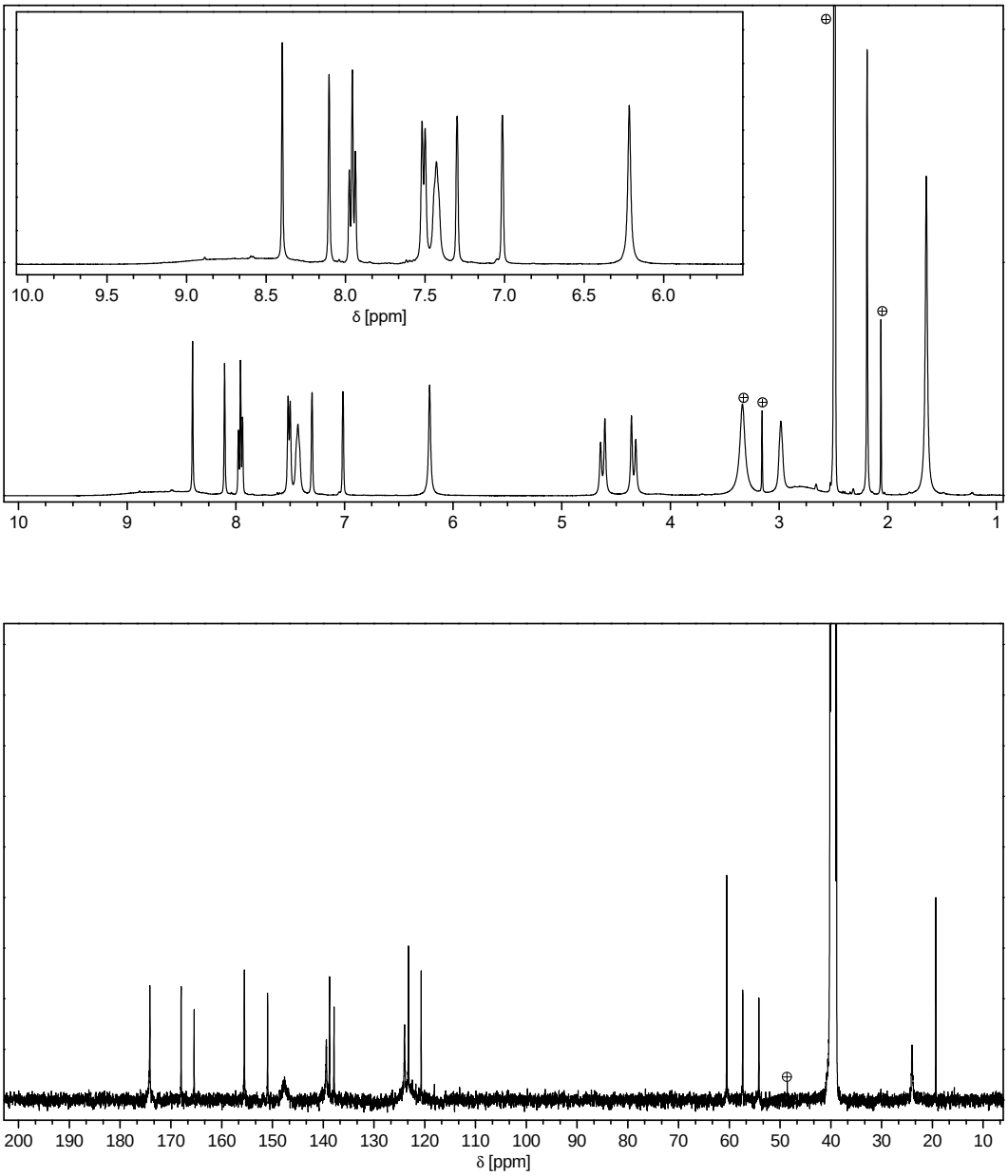


Figure S21: NMR spectra of $[Zn_2(tsc\text{-}hydra)(OAc)_2]$ in DMSO-$d_6$: (Top) $^1$H NMR; marked peak correspond to DMSO, methanol, acetonitrile and water. (Bottom) $^{13}C\{^1H\}$ NMR; marked peak corresponds to methanol. For notation of the ligand atoms cf. Fig. S10.

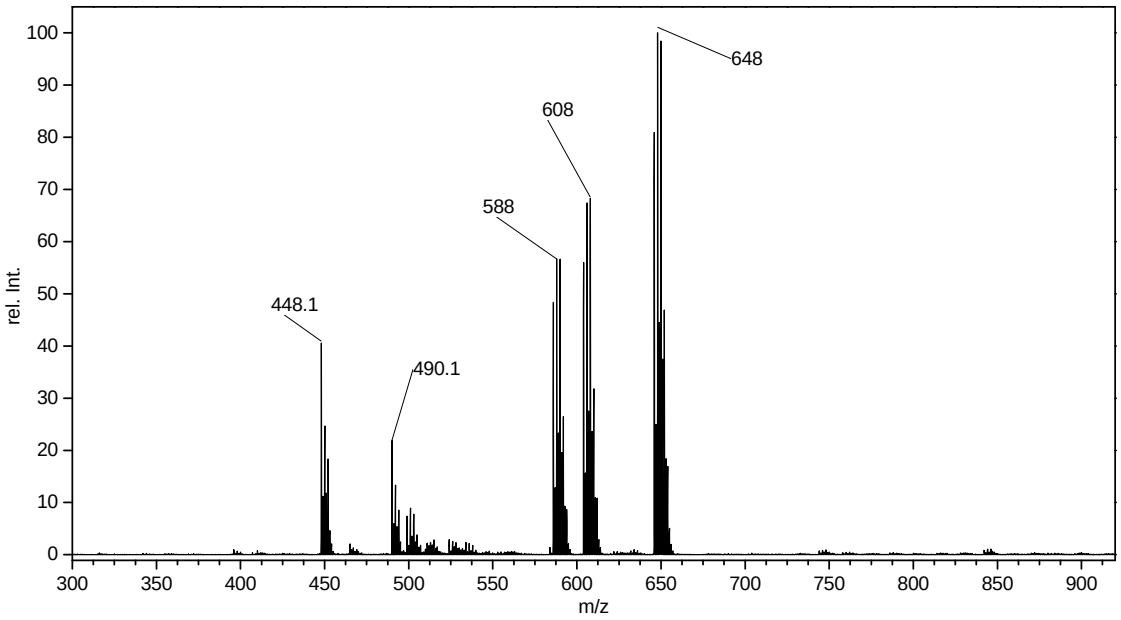


Figure S22: Mass spectrum in ESI positive mode of $[Zn_2(\text{tsc-hydra})(OAc)_2]$ in acetonitrile.

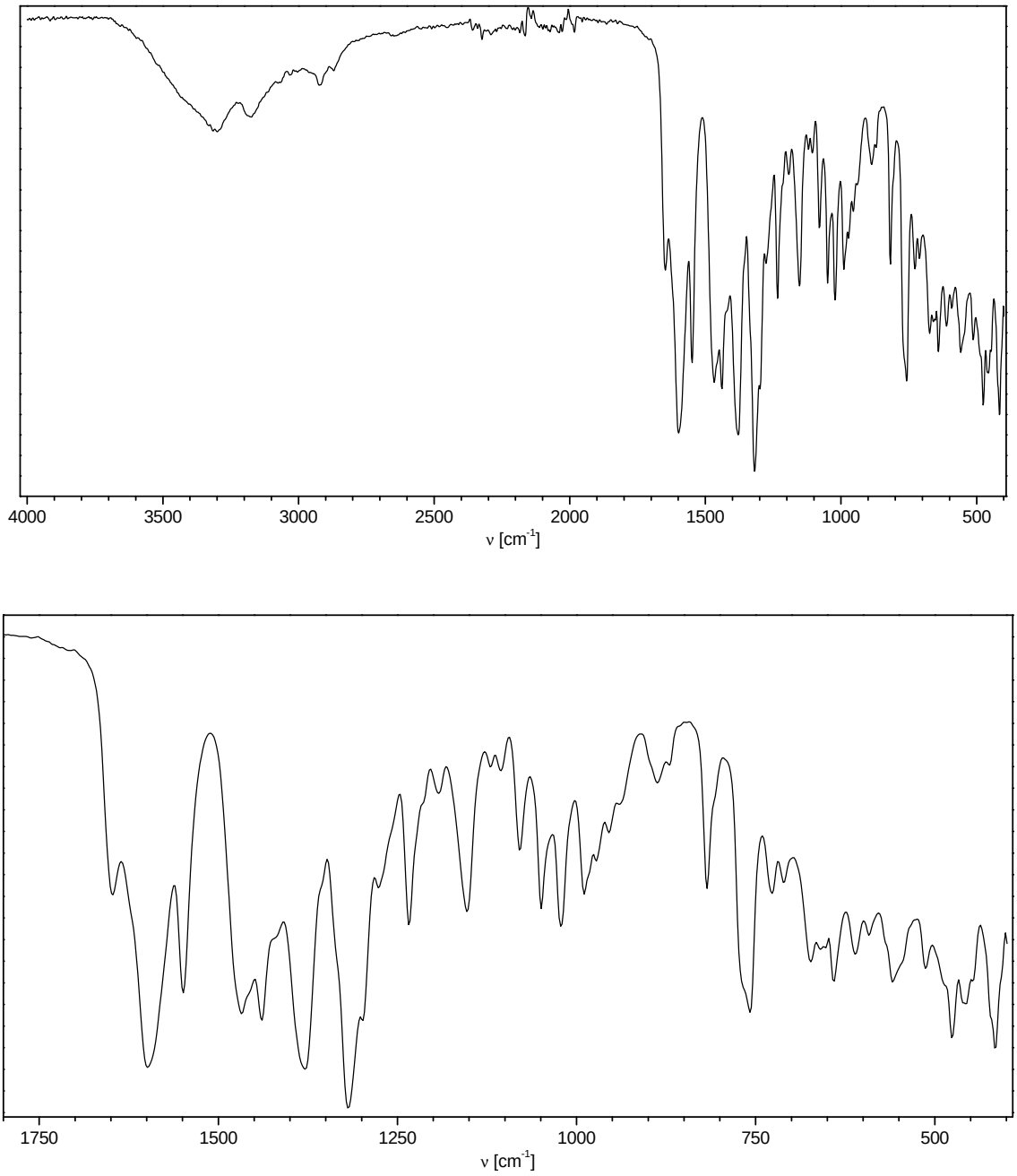


Figure S23: FT-IR spectra of $[Zn_2(\text{tsc-hydra})(OAc)_2]$: (Top) Overview range from 4000–400 $cm^{-1}$. (Bottom) Fingerprint region from 1800–400 $cm^{-1}$. List of the positions of vibrational bands (in $cm^{-1}$): 3309, 3180, 2921, 1649, 1598, 1550, 1466, 1438, 1378, 1319, 1296, 1276, 1232, 1193, 1152, 1104, 1079, 1051, 1019, 990, 971, 953, 937, 886, 820, 758, 728, 710, 676, 642, 614, 594, 561, 516, 477, 458, 415.

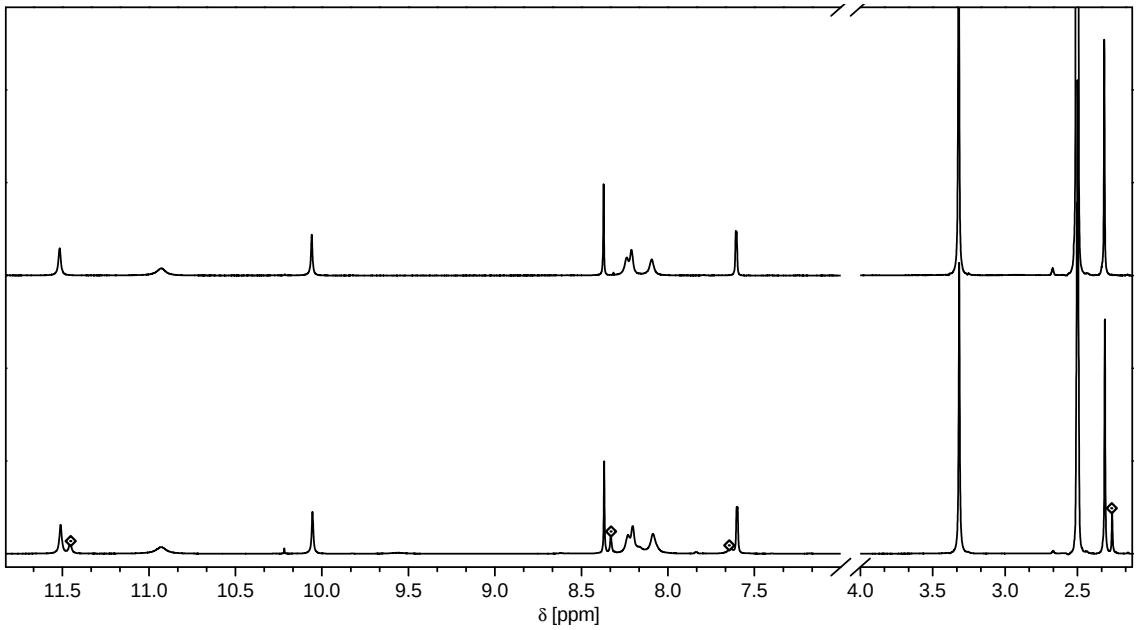


Figure S24: Comparison of the $^{1}$H NMR spectra of $H_2$tsc-difo before (lower line) and after purification by Soxhlet extraction with chloroform; both spectra were measured in DMSO-$d_6$; marked signals correspond to the symmetric byproduct.

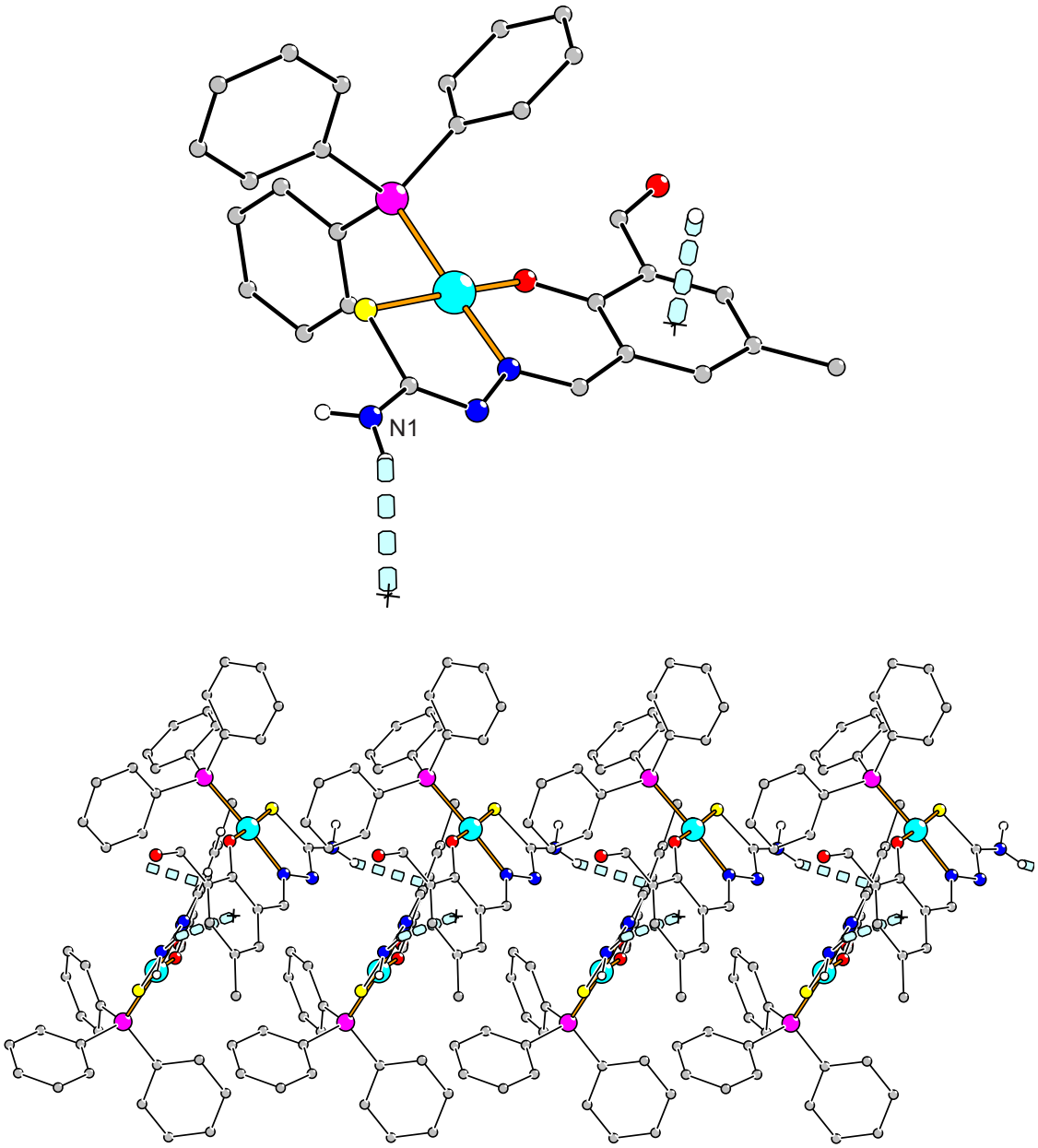


Figure S25: NH/$\pi$ interactions in the crystal structure of [Ni(tsc-difo)PPh$_3$]·2MeOH: (Top) Interactions at one complex molecule. (Bottom) Resulting zig-zag chain like arrangement along the [010] direction. Pertinent distances and angles: N1$\cdots$centroid 326 pm, H$\cdots$centroid 242 pm, N1–H$\cdots$centroid 162°.

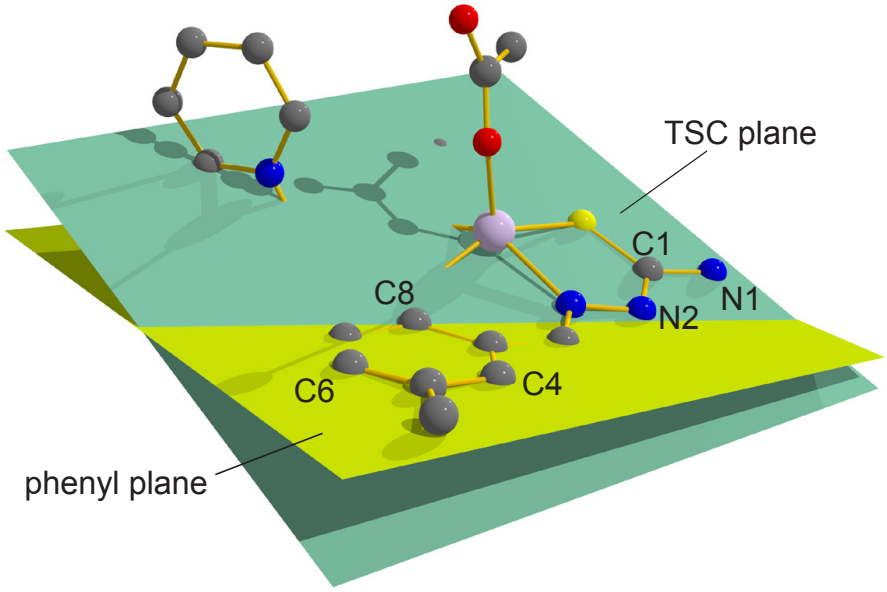


Figure S26: Representation of the mean planes for the thiosemicarbazone (N1, N2, C1) and the phenolate fragment (C4, C6, C8) in the crystal structure of $[Zn_2(tsc\text{-}hydra)(OAc)_2]\cdot MeCN\cdot H_2O$ indicating the rotation about the C2–C3 bond.

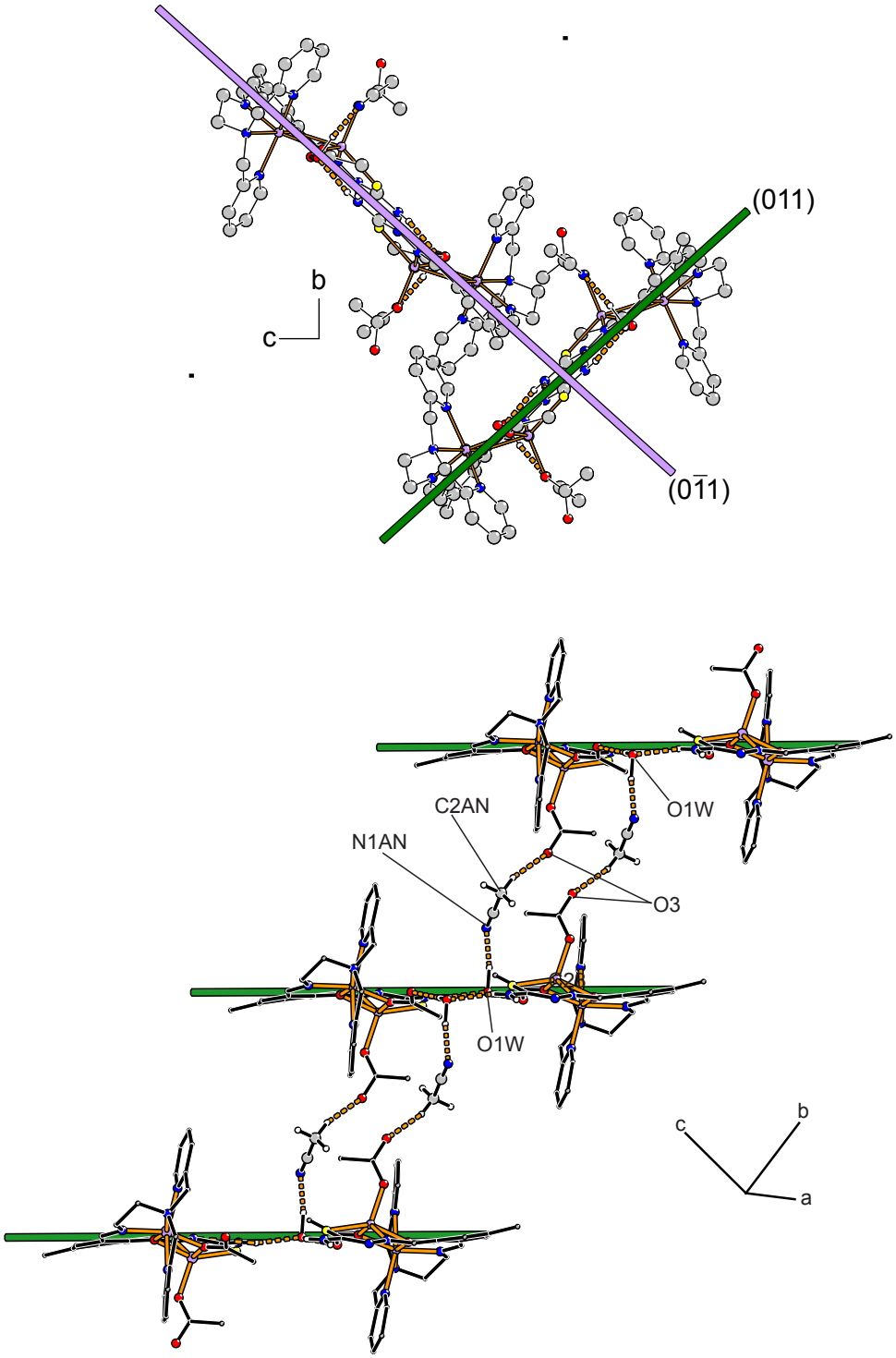


Figure S27: (Top) Representation of the two orientations of the hydrogen bonded chains along the [100] direction in the crystal structure of $[Zn_2(tsc\text{-}hydra)(OAc)_2]\cdot MeCN\cdot H_2O$. (Bottom) Interaction of the acetonitrile molecules with chains of the same orientation. Pertinent distances: O1W$\cdots$N1AN 298.4(9) and O3$\cdots$C2AN 318.2(9) pm.

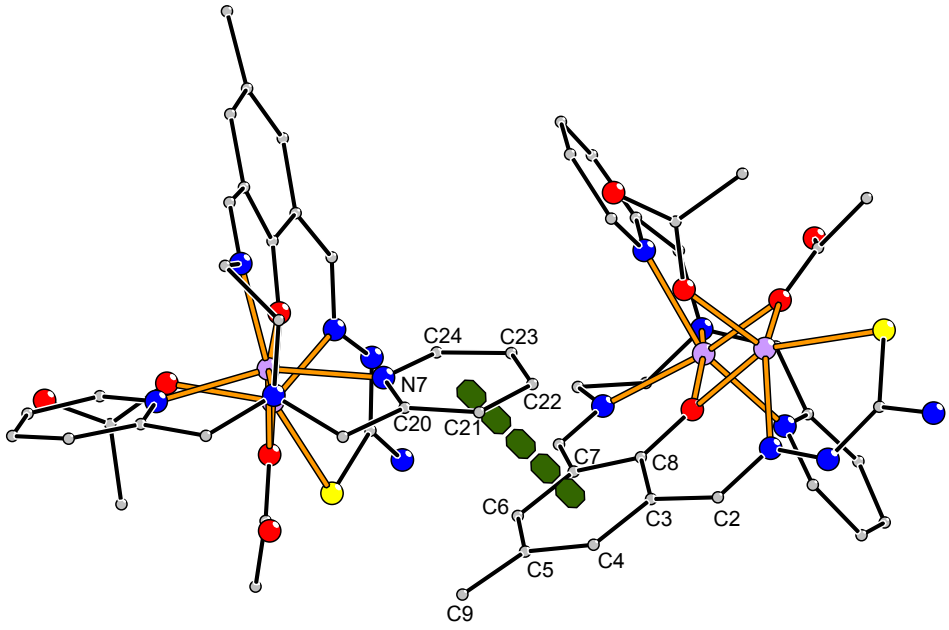


Figure S28: Representation of the $\pi$-$\pi$ interaction in the crystal structure of $[Zn_2(tsc\text{-}hydra)(OAc)_2]\cdot MeCN\cdot H_2O$. Pertinent data: centroid$\cdots$centroid distance 383.5 pm, shortest C–C contact 346 pm, angle between $\pi$ planes 19°.